A novel machine learning method to investigate the web crippling behaviour of perforated roll-formed aluminium alloy unlipped channels under interior-two flange loading

Zhiyuan Fang[a], Krishanu Roy[a,b*], Jinzhao Xu[a], Yecheng Dai[a], Bikram Paul[c], James B.P. Lim[a,b]

a Department of Civil and Environmental Engineering, The University of Auckland, New Zealand

b School of Engineering, The University of Waikato, New Zealand

c Department of Civil Engineering, National Institute of Technology, India

Abstract: This study presents a novel machine-learning model using the eXtreme Gradient Boosting (XGBoost) tool, for assessing the web crippling behaviour of perforated roll-formed aluminium alloy (RFA) unlipped channels (both fastened and unfastened) under interior-two-flange loading. A total of 1,080 data points were generated for training the XGBoost model, utilizing an elastoplastic finite element (FE) model that was validated against 30 experimental results from the literature. A comparison against the numerical failure loads was conducted, and it was found that the prediction accuracy of XGBoost model was 94%. When compared with Ramdom Forest and Linear Regression methods, it was found that the proposed XGBoost model performed better than both the beforementioned methods. The web crippling strengths obtained from the XGBoost model, tests, and finite element analysis (FEA) were utilized to evaluate the performance of current design rules from the American Iron and Steel Institute (AISI), Australian/New Zealand Standards (AS/NZS 1664.1; AS/NZS 4600:2018) and Eurocode (CEN 2007). It is shown that the current design rules are not reliable to predict the web crippling strength of perforated RFA unlipped channels. As a consequence of the parametric analysis, new web crippling strength and web crippling strength reduction factor formulae for perforated RFA unlipped channels were proposed. A reliability analysis was then

conducted, which confirmed that the proposed equations are capable of accurately predicting the ITF web crippling strengths of perforated RFA unlipped channels.

Keywords: Web crippling, eXtreme Gradient Boosting (XGBoost) tool, Aluminium alloy, Unlipped channels, Finite element analysis, Machine learning, Parametric analysis, Interior-two-flange loading.

1 Introduction

Thin-walled structures are widely used in building construction, storage racks, transmission towers, automotive, ships and aircraft [1-12]. Carbon steel, stainless steel, and aluminium are the most common materials used in the construction of thin-walled structures. As a sustainable building material, aluminium alloy has recently gained popularity in the construction industry [13-16], and roll-formed aluminium alloy (RFA) channels are being used as beam members. The inclusion of web perforations in such RFA channels is often required to facilitate the electrical and plumbing services. However, no research on the web crippling behaviour of perforated RFA unlipped channels when subjected to interior-two-flange (ITF) loading is available in the literature. Furthermore, current design standards i.e., American Iron and Steel Institute [17], the Australian and New Zealand Standards (AS/NZS 1664.1; AS/NZS 4600:2018) [18-19], as well as the Eurocode (CEN 2007) [20], do not include recommendations for perforated RFA unlipped channels under ITF loading. In this paper, a novel machine learning model using the eXtreme Gradient Boosting (XGBoost) tool is trained based on the validated elasto-plastic finite element (FE) model to investigate the interior-two flange (ITF) web crippling behaviour of perforated RFA unlipped channels (see Fig.1) and new design equations were proposed.

Limited research is available in the literature for the web crippling performance of perforated RFA unlipped channels. Previous research studies [21-28] have mainly focused on RFA lipped channels. The effect of lip on the stiffness of the flange, which would normally increase the web crippling strength, was often ignored, although there are few studies available in the literature which demonstrates the effect of lip and folded flanges on the stiffness of channel sections [29-32]. Furthermore, research into the effect of web holes on aluminium

alloy sections under web crippling is very limited. As a result, a thorough investigation on the web crippling behaviour of perforated RFA unlipped channels is required.

The web crippling behaviour of roll-formed carbon steel (RFCS) sections has been studied extensively. Bhakta et al. [33] investigated the enhancement of web crippling capacity from fastened supports of different RFCS sections. Similarly, Cain et al. [34] and Gerges and Schuster [35] examined the effects of fastened flanges on the web crippling behaviour. The web crippling strength of fastened sections was found to be over 30% higher than that of sections with unfastened flanges. These findings are in line with most of the recent results reported in the literature [36-49]. The design calculation methods from the standards are discussed in the literature [36-41], however, the proposed Direct Strength Method in the literature [36-41] are only available in predicting the web crippling strength of plain sections; Uzzaman et al. [42-49] therefore proposed new equations in the form of reduction factor equation to predict the web crippling strength of perforated cold-formed steel channels based on experimental and numerical studies.

Machine Learning (ML) is a useful method for identifying useful data features [50], and the use of ML to predict the trend of data has gained popularity in recent times [51-56]. XGBoost is an effective ML tool, which is used for eXtreme Gradient Boosting. Compared with traditional gradient boosting algorithms, XGBoost is much faster while classifying and training the data.

This research has therefore proposed a XGBoost framework for investigating the ITF web crippling strength of perforated RFA unlipped channels. A nonlinear elasto-plastic finite element (FE) model was developed and validated against the experimental data available in the literature. A total of 1,080 data points were obtained for training the XGBoost utilizing the validated FE model. When the XGBoost predictions were compared to the web crippling

strengths of perforated RFA unlipped channels determined from the AISI 2016 [17] and AS/NZS 2018 [19], AS/NZS 1997 [18], and CEN 2007 [20], it was found that the XGBoost performs better. Additionally, the prediction accuracy of XGBoost was checked against the results of other ML methods, i.e., Random Forest and Linear Regression, and it was found that XGBoost outperformed the other two methods when predicting the web crippling strength of RFA unlipped channels. Based on the XGBoost output data, a parametric study was carried out and design equations for the reduced web crippling strength of RFA channels were proposed. Furthermore, a reliability analysis of the proposed equations confirmed that the proposed equations could closely predict the (reduced) ITF web crippling strength of RFA unlipped channels.

2 Summary of experimental results reported by Fang et al. [57]

Fang et al. [57] conducted 30 new experimental tests on perforated RFA lipped channels under ITF loading condition. The size and location of web perforations were altered to determine its influence on the web crippling behaviour of such channels. The test specimens had web holes placed at the centre and also offset longitudinally from the bearing plate. The specimens were labelled in such a manner that the label stated the nominal dimensions of the web, bearing length, hole position, hole size, and flange type. For instance, the label "ITF240-N50-DH-A0.6-FR" can be defined as follows: “ITF” represents the study's web crippling loading case; "240" denotes the nominal web depth in millimetres (d=240 mm); "N50" denotes the bearing's length in millimetres (N=50 mm); the abbreviations "NH", "DH", and "OH" denote the web hole status. "NH" indicates that there are no web holes, whereas "DH" and "OH" indicate that the web has a down hole and an offset hole, respectively; "A0.6" denotes the ratio of the hole diameter to the total web depth (a/h=0.6). The final two notations "FR" and "FX" denote sections with unfastened and fastened flanges, respectively.

The test results of Fang et al. [57] were used in the current study to validate the FE models developed herein, as described in the following section. More details of the experiments and its results can be found in Fang et al. [57].

3 Advanced finite element analysis (FEA)

3.1 Development of the FE model

The experimental behaviour was simulated numerically through a nonlinear nonlinear elasto-plastic FE model, which was developed using the software ABAQUS [58]. The material properties obtained from the tensile coupon tests [57] were input into the FE models. S4R shell elements (having a mesh size of 5 mm × 5 mm) were used in the FE modelling to model the RFA unlipped channels, and rigid quadrilateral shell elements (R3D4) were used to model the endplates. Fig.2 illustrates the details of FE meshing and the boundary conditions of the FE model.

The interface of bearing plate and the channel was modelled using the surface-to-surface contact option available in ABAQUS [58]. The target surface was the bearing plate, whereas the contact surface was selected to be the channel surface. No penetration of the two contact surfaces was permitted. The vertical load was applied to the channels through the reference node of the top bearing plate by means of displacement control load application procedure. Similar FE modelling techniques were also employed by Chi et al. [59], Chen et al. [60-63], Roy et al. [64-68], Fang et al. [69-74] and Yao and Li [75], and it should be noted that Fang et al. [74] have demonstrated that such modelling methods are feasible for simulating both unlipped and lipped channels subjected to web crippling.

The effects of initial geometric imperfections and residual stresses can be neglected in the finite element models of light gauge steel sections subject to web crippling. In the web crippling study, the expected buckling modes exhibit stable post buckling behaviour which

126 significantly reduces its effects on imperfection sensitivity, and meanwhile, the stocky channel
127 sections with restraints at both ends also reduce the imperfection effects. This is already
128 confirmed by a number of research studies [76-79]. In these studies [26,28,42-46,74], the
129 researchers conducted both the experimental and numerical investigations on the web crippling
130 behaviour of thin-walled structures, where the ratio of channel length to the web depth was
131 around 3. This ratio has been adopted in the parametric study of this paper. Therefore, the
132 effects of initial geometric imperfections and residual stresses were not considered in the FE
133 models developed in this study.

134 *3.2 FEM validation*

135 In total, 30 experimental results from Fang et al. [57] were used to validate the FE model,
136 and the comparison results of FEA and tests are reported in Table 1. The mean values of the
137 ratio of experimental to FEA strengths (P_{EXP}/P_{FEA}) are 1.06 and 1.04, respectively for
138 unfastened and fastened sections, with coefficients of variation (COVs) of 0.02 and 0.03,
139 respectively. Fig.3 depicted the numerical and experimental ITF web crippling failure modes
140 of the investigated channels. In terms of load-vertical displacement behaviour, the numerical
141 results were found to be very close to the experimental results (see Fig.3). Therefore, the
142 developed FE models could closely predict the ITF web crippling strength of perforated RFA
143 channels.

144 # 4 Current design rules

145 *4.1 Web crippling strength for plain channels*

146 *4.1.1 AS/NZS 1664.1 [18]*

147 The nominal web crippling strength ($P_{AS/NZS1664}$) of RFA unlipped channels subjected
148 ITF loading could be calculated using Equation 1 as below.

149 $$P_{\mathrm{AS/NZS1664}} = \frac{t^2 \sin\theta\left(0.46 f_y + 0.02\sqrt{E f_y}\right)\left(N + C_{w1}\right)}{C_{w3} + r_i\left(1-\cos\theta\right)} \quad (1)$$

150 where, C_{w1}=140mm; C_{w2}=33mm; C_{w3}=10mm; θ=90°.

151 *4.1.2 Eurocode [20]*

152 The ITF web crippling strength (P_{CEN}) of RFA unlipped channels can be determined by
153 Equation 2 available in Eurocode [20].

154 $$P_{\mathrm{CEN}} = \alpha t^2 \sqrt{f_y E}\left(2.4 + \left(\frac{\theta}{90}\right)^2\right)\left(1 - 0.1\sqrt{\frac{r_i}{t}}\right)\left(0.5 + \sqrt{\frac{0.02N}{t}}\right) \quad (2)$$

155 where, α represents the coefficient for several local loads as well as for support categories of
156 the cross-sections.

157 *4.1.3 AISI&AS/NZS 4600:2018 [17,19]*

158 The unified web crippling design strength ($P_{\mathrm{AISI\&AS/NZS}}$) of RFCS plain sections could be
159 determined by using Equation 3 of AISI&AS/NZS 4600:2018 [17,19].

160 $$P_{AISI\&AS/NZS} = C t^2 f_y \sin\theta\left(1 - C_w\sqrt{\frac{h}{t}}\right)\left(1 - C_r\sqrt{\frac{r}{t}}\right)\left(1 + C_l\sqrt{\frac{N}{t}}\right) \quad (3)$$

161 where, C, N, C_{r}, C_{l} and C_{w} represent equation coefficients.

162 *4.2 Web crippling strength reduction factor*

163 Due to the absence of design rules for the strength reduction factor of roll-formed
164 aluminium alloy channel sections, the equations proposed by Uzzaman et al. [42-44] were
165 employed in this study. It should be noted that these equations [42-44] are for roll-formed
166 carbon steel perforated lipped channels and are limited to $h/t \leq 156$, $N/t \leq 84$, $N/h \leq 0.63$ and
167 $a/h \leq 0.8$. Moreover, it is important to note that the N/h ratio was not included in the design
168 equations of Uzzaman et al. [42-44].

5 eXtreme Gradient Boosting (XGBoost)

5.1 Overview

eXtreme Gradient Boosting (XGBoost) database is a collection of algorithms based on the boosting framework. The loss function of XGBoost performs a more accurate second order Taylor expansion on the error component throughout the optimisation method of the algorithm. Parallel selection is normally used to determine the appropriate subtree splitting features and eigenvalues for each weak learner, similar to the process of decision tree construction. Prior to parallel selection, all feature values are sorted and grouped to simplify the previously described parallel selection. This algorithm selects the proper group size for the grouped features.

5.2 Cross validation

Overfitting happens frequently during the training phase, which indicates that the model can accurately match the training data but cannot reliably predict the data outside of the training set. Isolating a portion of the training data from the validation data is a standard practice. Cross-validation, also known as round robin validation, is a method of assessing a model against its validation data. In order to develop K models, the data in this study was divided into K groups (K-Fold) and a validation set for each subset of data was created, while utilising the rest of the K-1 subset data as the training set. To calculate the cross-validation error, the validation set was divided into K models, and the final MSE (Mean Squared Error) was summed and averaged.

5.3 Data training

The data obtained from the validated FE models were used to train the XGBoost algorithm. Prior to normalisation, the input and output data points were formulated as follows:

$$\text{Input} = \left\{ b_w, b_f, r, t, N, a, x, n_h, f_y, \right\} \tag{4}$$

192 $$\text{Output} = \{P_p\} \quad (5)$$

193 To minimise the over-fitting of the data, this study employed a learning rate, and used
194 the subsample method. The available data was split into two groups including: training and
195 testing set. A total of 1,080 data vectors were utilised in this study. The database was randomly
196 divided into training and testing data sets as a ratio of 70% and 30%, respectively.

197 *5.4 Performance evaluation*

198 To evaluate the prediction accuracy of the ML algorithm, the absolute percentage error
199 (Err_i (%)), correlation coefficient (R^*), mean absolute error (MAE), and the root mean square
200 error (RMSE) were determined. The following are the formulae for determining each of these
201 parameters:

202 $$\text{Err}_i(\%) = \frac{|y_i - t_i|}{t_i} \times 100 \quad (6)$$

203 $$R^* = \frac{\sum_{i=1}^{N}(y_i - \overline{y_i})(t_i - \overline{t_i})}{\sqrt{\sum_{i=1}^{N}(y_i - \overline{y_i})^2 \sum_{i=1}^{N}(t_i - \overline{t_i})^2}} \quad (7)$$

204 $$RMSE = \sqrt{\frac{\sum_{i=1}^{N}(t_i - y_i)^2}{N}} \quad (8)$$

205 $$\text{MAE} = \frac{1}{N}\sum_{i=1}^{N}|y_i - t_i| \quad (9)$$

206 where, t_i and y_i represent the real as well as prediction output values, respectively, and $\overline{t_i}$ and
207 $\overline{y_i}$ represent the averages of the real and predicted outputs, respectively. N denotes the data
208 series.

209 The prediction accuracy of XGBoost algorithm was evaluated using the correlation
210 coefficient (R*), root mean square error (RMSE), and mean absolute error (MAE). The R*

211 value indicates how well the proposed formulation can predict the data. The root mean square
212 error is also referred to as the cost function, and it plays a significant role in the learning process
213 of a machine learning algorithm. The root means square error (RMSE) and the mean absolute
214 error (MAE) both quantify the accuracy and goodness of the data fit. A good prediction model
215 has lower RMSE and MAE values, which are close to having an R^* value of 1.00. The
216 performance metrics for both training and testing data sets were determined using a 70%-30%
217 training-testing split of the entire database. Cross-validation was carried out using the same
218 training data as what was used to evaluate the measures (see Table 2).

219 As shown in Table 2 and in Fig.4, the R^* value obtained from the training set is the
220 highest (0.9999), while the MAE and RMSE values are 0.0057 and 0.0032, respectively.
221 Similarly, in the XGBoost model, the R^*, RMSE, and MAE values for the testing set are 0.9969,
222 0.5340 and 0.2442, respectively. This indicates that the XGBoost model can predict the web
223 crippling strength of RFA channels with high accuracy. Besides, the performance of XGBoost
224 model was also compared with that of Random Forest and Linear Regression techniques. As
225 demonstrated in Table 3, the XGBoost model significantly performed better than the Random
226 Forest and Linear Regression Analysis.

227 *5.5 Comparison of results obtained from the machine-learning methods with the current design*
228 *standards*

229 The machine-learning method's prediction accuracy was assessed by comparing its
230 results to the current design strengths in accordance with the AS/NZS 1664 [18], CEN 2007
231 [20], and AISI & AS/NZS [17,19]. The machine-learning method (XGBoost model) achieved
232 high prediction accuracy for training (R^*=0.9998, MSE=0.0057, MAE=0.0033) and testing
233 (R^*=0.9969, MSE=0.5341, MAE=0.2442) data sets. In Table 4, the mean absolute percentage
234 errors for web crippling capacity of unfastened sections obtained from the FEA results are

71.5%, 83.2%, 63.2% and 5.9%, respectively, when compared to the design strengths obtained from the AS/NZS 1664 [18], CEN 2007 [20], and AISI & AS/NZS [17,19]. The mean absolute percentage errors for fastened sections are 68.0%, 81.1%, 68.1% and 6.4%. The results show that the design strengths calculated from the AS/NZS 1664 [18], CEN 2007 [20], and AISI&AS/NZS [17,19] are almost 30% lower than the FEA and XGBoost results. In comparison to the calculation results of the existing design standards, both the FEA and XGBoost results could more precisely predict the web crippling strength of perforated RFA unlipped channels.

6 Parametric study

A comprehensive parametric study was carried out utilizing the validated XGBoost model to determine the effects of hole size, hole location, section thickness, and the length of bearing plate on the web crippling strength of perforated RFA unlipped channel under ITF loading. The *a/h* ratio was adjusted between 0 and 0.8, with a step increment of 0.2. Thickness of the section (*t*) was varied from 1 to 4mm, while the radius of the corner (*r*) was altered between 2 and 6mm, as shown in Table 5. The effect of bearing lengths (*N*): 50, 75, and 100mm were studied (see Table 5).

6.1 Effect of r/t, N/t, h/t and flange types

Figs.5(a-c) present the effects of ratios *r/t*, *N/t* and *h/t* on the dimensionless web crippling strength of RFA unlipped channels. The downward trend of dimensionless strength of the investigated channels was observed when the *r/t* and *h/t* ratios were increased. On the other hand, the web crippling strength increased when the N/t ratio increased from 0.21 to 0.63. From Fig.5(d), it can be seen that P_n for RFA unlipped channels with fastened flanges are typically greater than those with unfastened flanges, with a mean difference of 34.9%.

6.2 Effects of a/h, N/h and x/h ratios on R

Fig.6(a) and Table 5 show the influence of *a*/*h* ratio on the value of *R*. Fig.6(a) shows a decreasing trend in the web crippling strength reduction factors as the *a*/*h* ratio increased from 0.2 to 0.8. On the one hand, *R* values for offset-hole sections with unfastened and fastened flanges were comparable, but the mean value of *R* for these two groups of sections is significantly different, decreasing from 0.93 to 0.54 and from 0.95 to 0.67, respectively, as the *a*/*h* ratio increased from 0.2 to 0.8. On the other hand, a rather minor variation in *R* value was detected between the unfastened and fastened flanges with centred web holes. As reported in Table 5, the mean value of *R* was reduced from 0.95 to 0.61 for centred hole sections with unfastened flanges. Similarly, when the *a*/*h* ratio was raised from 0.2 to 0.8, the value of *R* for sections with fastened flanges dropped from 0.96 to 0.60.

As the *N*/*h* ratio was increased from 0.21 to 0.75 for channels with centred web holes, the mean value of *R* for channels with unfastened and fastened flanges were decreased from 0.84 to 0.80 and from 0.80 to 0.84, respectively. *R* values increased from 0.73 to 0.75 and from 0.80 to 0.86 for unfastened and fastened flanges of channels with offset web holes, respectively.

The mean value of *R* for channels with unfastened and fastened flanges ranged between 0.68 and 0.92 and between 0.78 to 0.95, respectively, when the *x/h* ratio was adjusted between 0.01 and 0.50. As can be seen from Fig.6(c), there is a noticeable variation in the trend of *R* for the RFA unlipped channel with un-fastened and fastened flanges having offset web holes with varying *a*/*h* ratios.

Fig.6(d) and Table 5 show the effect of fastened flanges on the value of *R* when the *a/h* ratio and hole location were varied. As can be observed from Fig.6(d) and from Table 5, the mean value of *R* for channels varied slightly. The value of *R* for channels with unfastened flanges is comparable to that of channels with fastened flanges, whereas the mean values of *R*

for unfastened sections with offset web holes are greater than those for fastened sections with offset web holes (by 11.1% on average).

7 Proposed design equations and reliability analysis

Based on the results of XGBoost model, design equations in the form of web crippling strength and web crippling strength reduction factors are proposed. The proposed equations have limits of the parameters as: $h/t \leq 295$, $N/t \leq 100$, $R/t \leq 6.0$, $N/h \leq 0.75$ and $a/h \leq 0.8$. The ranges of h/t, N/t, and N/h were increased relative to the proposed carbon steel equations of Uzzaman et al. [42-44].

7.1 Proposed equations

The design equations for calculating the web crippling strength (P_{prop}) and web crippling strength reduction factor (R_{prop}) of RFA unlipped channel sections subjected to ITF loading are proposed as follows:

$$P_{prop} = Ct^2 f_y (1 - C_R\sqrt{\frac{r}{t}})(1 + C_N\sqrt{\frac{N}{t}})(1 - C_h\sqrt{\frac{h}{t}}) > 0 \quad (10)$$

For sections with a centred web hole,

$$R_{prop} = \alpha - \gamma\frac{a}{h} + \lambda\frac{N}{h} \leq 1 \quad (11)$$

For sections with offset web holes,

$$R_{prop} = \beta - \mu\frac{a}{h} + \zeta\frac{N}{h} + \xi\frac{x}{h} \leq 1 \quad (12)$$

where, the recommended values for C, C_R, C_N and C_h are listed in Table 6. The values of α, γ, λ, β, μ, ζ and ξ represent the coefficient values which are presented in Table 7 for each type of section.

By comparing the proposed design strengths with the FE strengths and the failure strengths calculated from the equations from Uzzaman et al. [42-44], it was found that the prediction accuracy of the proposed equations is much better. The reduced web crippling strength calculated using the proposed equations are highly predictive of the FE strengths, as shown in Table 8, and the mean values of the ratios of P/P_{prop}, R/R_{prop} are both close to 1, demonstrating that the (reduced) ITF web crippling strength of RFA unlipped channels could be closely predicted by the proposed design equations.

7.2 Reliability analysis

To assess the performance accuracy of proposed design equations, a reliability study was conducted using the technique described by Hsiao et al. [80]. Any proposed design equation is considered to be reliable if its reliability index (β') is more than or equal to the target reliability index of 2.5, according to the American standard (AISI S100-16 [17]). The reliability indices of the proposed equations are higher than the target index of 2.5, (see Table 9). This confirms that the proposed design equations could predict the ITF web crippling strength of RFA unlipped channels with high degree of precision.

8 Conclusions

A novel machine-learning model using the XGBoost tool was developed to investigate the ITF web crippling behaviour of perforated RFA unlipped channels. A nonlinear elasto-plastic FE model was developed and validated against the experimental results available in literature. To train the XGBoost model, a total of 1,080 data points were created using the validated FE model. The XGBoost predictions were close to the numerical failure loads, being conservative by only 6% for unlipped channels with unfastened flanges and by 7% for sections with fastened flanges. The training process and the performance of the proposed XGBoost model were also compared with that of Random Forest and Linear Regression techniques, and

it was found that the XGBoost model outperformed the other two techniques. The XGBoost results were then compared to the design strengths calculated from the Australian/New Zealand standard (AS/NZS 1664.1; AS/NZS 4600:2018), American Iron and Steel Institute (AISI), and Eurocode standards (CEN 2007). The developed XGBoost model was found to outperform the existing design standards. The design strengths in accordance with the AS/NZS 1664.1, AISI&AS/NZS 4600:2018, and CEN 2007 were found to be excessively conservative by 95.5%, 65.3%, and 34.1% for aluminium alloy unlipped channels with unfastened flanges, respectively, and conservative by 34.9%, 21.7%, and 7.3% for channels with fastened flanges.

Finally, using the XGBoost output, a parametric study was conducted, and it was found that the web crippling strength is sensitive to the changes in geometrical parameters such as hole size, hole location, section thickness, and the length of bearing plate. Using the XGBoost predictions, new design equations for web crippling strength and web crippling strength reduction factor were proposed. A reliability analysis was also performed; the results of which confirmed that the proposed design equations could be used to predict the web crippling strength of perforated RFA unlipped channels subjected to ITF loading condition.

Acknowledgements

The authors greatly acknowledge for the support of University of Auckland for providing the high-speed computing machines.

References

[1] M. Wan, M. Chen, Seismic performance analysis of Mongolian yurt rigid frames with cold-formed C-shaped steel, Prog. Steel Build. Struct. 22 (3) (2020) 12-21.

[2] W. Gao, J. Wan, S. Liu, A stability design theory for the steel members using asymmetric thin-walled open-sections, Prog. Steel Build. Struct. 23 (5) (2021) 53-62.

[3] X. Chen, J. Wang, S. Guo, Hysteretic behavior of the endplate joints for concrete-filled thin-walled steel tubular frames, Prog. Steel Build. Struct. 23 (7) (2021) 97-104.

[4] Y. Yang, Z. Liu, Simplified formulae for the critical distortional buckling stress of C-section columns with or without V-stiffeners at the flange, Prog. Steel Build. Struct. 23 (6) (2021) 71-77.

[5] J. Yang, W. Wang, The influence of high temperature creep on the fire resistance of cold-formed steel columns, Prog. Steel Build. Struct. 23 (7) (2021) 67-75.

[6] J. Zhang, M. Sun, Numerical simulation and load bearing capacity study for high strength cold-formed steel open section columns after fire exposure, Prog. Steel Build. Struct. 23 (9) (2021) 67-71.

[7] D.T. Phan, S.M. Mojtabaei, I. Hajirasouliha, J. Ye, J.B.P Lim. Coupled Element and Structural Level Optimisation Framework for Cold-Formed Steel Frames, J. Constr. Steel Res. 49 (2019) 69-83.

[8] S.M. Mojtabaei, M.Z. Kabir, I. Hajirasouliha, M. Kargar. Analytical and experimental study on the seismic performance of cold-formed steel frames, J. Constr. Steel Res. 143 (2018) 18-31.

[9] S.M. Mojtabaei, J. Becque, I. Hajirasouliha. Local buckling in cold-formed steel moment resisting bolted connections: behaviour, capacity and design, J. Struct. Eng. 146 (2020) 04020167.

[10] D.T. Phan, S.M. Mojtabaei, I. Hajirasouliha, T. L. Lau, J.B.P Lim. Design and optimisation of cold-formed steel sections in bolted moment connections considering bimoment, J. Struct. Eng. 146 (2020) 04020153.

[11] S.M. Mojtabaei, J. Becque, I. Hajirasouliha, Behavior and Design of Cold-Formed Steel Bolted Connections Subjected to Combined Actions, J. Struct. Eng. 147 (2021) 04021013.

[12] H. Liang, K. Roy, Z. Fang, J.B.P. Lim, A Critical Review on Optimization of Cold-Formed Steel Members for Better Structural and Thermal Performances. Buildings. 12 (2022) 34.

[13] W.S. Miller, L.Z. Zhuang, J. Bottema, A.J. Wittebrood, D.S. Peter, A. Haszler, A. Vieregge, Recent development in aluminium alloys for the automotive industry. Mater. Sci. Eng. 280 (1) (2000) 37–49.

[14] X. Guo, S. Zong, Z. Cheng, L. Zhu, X. Zhou, State-of-the-art of the research on corrosion resistance of aluminum alloy structures, Prog. Steel Build. Struct. 23 (6) (2021) 1-12.

[15] B. Li, Y. Wang, X. Zhi, Z. Wang, H. Yuan, Y. Ouyang, A review on the research of the 7××× series high strength aluminum alloys as structural material in China, Prog. Steel Build. Struct. 23 (7) (2021) 1-10.

[16] X. Hu, Y. Cheng, X. Chen, Research on the performance of domestic 701 aluminum alloy l-shaped members under axial compression, Prog. Steel Build. Struct. 23 (11) (2021) 63-71.

[17] American Iron and Steel Institute (AISI). North American Specification for the Design of Cold-formed Steel Structural Members AISI S100-16; 2016.

[18] Australian/New Zealand Standard (AS/NZS). Aluminium Structures Part 1: Limit State Design. AS/NZS 1664.1: 1997, Sydney, Australia, 1997.

[19] Australia/New Zealand Standard (AS/NZS). Cold-Formed Steel Structures, AS/NZS 4600:2018. Standards Australia/ Standards New Zealand; 2018.

[20] European Committee for Standardization (CEN), Design of Aluminium Structures - Part 1.4 vol. 9, Cold-formed structural sheeting, Eurocode, Brussels, Belgium, 2007.

[21] F. Zhou, B. Young, Web crippling of aluminium alloy channels with flanges restrained. Thin-Walled Struct. 148 (2020) 106576.

[22] H. Alsanat, S. Gunalan, P. Keerthan, H. Guan, C. Baniotopoulos, Fastened Aluminium-Lipped Channels Subjected to Web Crippling under Two-Flange Loading Conditions: Experimental Study. J Struct Eng. 146 (4) (2020) 04020023.

[23] H. Alsanat, S. Gunalan, H. Guan, P. Keerthan, J. Bull, Experimental study of aluminium lipped channels subjected to web crippling under two flange load cases. Thin-Walled Struct. 141 (2019) 460-476.

[24] H. Alsanat, S. Gunalan, K. Poologanathan, H. Guan, Web crippling investigations of aluminium lipped channel sections under one-flange loading conditions. Thin-Walled Struct. 166 (2021) 108025.

[25] H. Alsanat, S. Gunalan, K. Poologanathan, H. Guan, Web crippling capacities of fastened aluminium lipped channel sections subjected to one-flange loading conditions. Struct. 33, (2021) 1754-1763.

[26] Z.Y. Fang, K. Roy, Q. Ma, A. Uzzaman, J.B.P. Lim, Application of deep learning method in web crippling strength prediction of cold-formed stainless steel channels under end-two-flange loading, Struct. 33 (2021) 2903-2942.

[27] K. Roy, T. C. H. Ting, H. H. Lau, R. Masood, R. Alyousef, H. Alabduljabbar, A. Alaskar, J.B.P. Lim, Cold-Formed Steel Lipped Channel Section Columns Undergoing Local-Overall Buckling Interaction. International Journal of Steel Struct. 21 (2) (2021) 408–429.

[28] Z.Y. Fang, K. Roy, Y. Dai, J.B.P. Lim, Effect of holes on end-two-flange web crippling behaviour of roll-formed aluminium alloy unlipped channels through experimental test, numerical simulation and deep learning. Thin-Walled Struct. (Under review)

[29] K. Roy, H. H. Lau, Z.Y. Fang, A. M. M. Ahmed, J. B.P. Lim, Axial capacity of back-to-back built-up cold-formed stainless steel unlipped channels-Numerical investigation and parametric study. Steel Compos. Struct. 40(5) (2021) 761-780.

[30] K. Roy, H. H. Lau, Z.Y. Fang, A. M. M. Ahmed, J. B.P. Lim, Axial capacity of back-to-back built-up cold-formed stainless steel unlipped channels-Numerical investigation and parametric study. Steel Compos. Struct. 40(5) (2021) 761-780.

[31] J. Ye, S. M. Mojtabaei, I. Hajirasouliha, P. Shepherd, K. Pilakoutas, Strength and deflection behaviour of cold-formed steel back-to-back channels, Eng. Struct. 177 (2018) 641–654.

[32] A.M. Yousefi, B. Samali, I. Hajirasouliha, Y. Yu, G. C. Clifton, Unified design equations for web crippling failure of cold-formed ferritic stainless steel unlipped channel-sections with web holes", J. Build. Eng. 45 (2021) 103685.

[33] B.H. Bhakta, R.A. LaBoube, W.W. Yu, The effect of flange restraint on web crippling strength, Final Report, Civil Engineering Study vols. 92–1, University of MissouriRolla, Rolla, Missouri, U.S.A, 1992.

[34] D.E. Cain, R.A. LaBoube, W.W. Yu, The effect of flange restraint on web crippling strength of cold-formed Steel Z-and I-sections, Final Report, Civil Engineering Study vols. 95–2, University of Missouri-Rolla, Rolla, Missouri, U.S.A, 1995.

[35] R.R. Gerges, R.M. Schuster, Web crippling of single web cold-formed steel members subjected to End-One-Flange loading, Proc of 14th International Specialty Conference on Cold-Formed Steel Structures, St. Louis, Missouri, U.S.A, 1998.

[36] L. Sundararajah, M. Mahendran, P. Keerthan, Experimental studies of lipped channel beams subject to web crippling under two-flange load cases, J. Struct. Eng. 142 (2016) 04016058.

[37] S. Gunalan, M. Mahendran, Web crippling tests of cold-formed steel channels under two flange load cases, J. Constr. Steel Res. 110 (2015) 1-15.

[38] V.V. Nguyen, G.J. Hancock, C.H. Pham, Consistent and Simplified Direct Strength Method for Design of Cold-Formed Steel Structural Members under Localized Loading. ASCE J. Struct. Eng. 146 (2020).

[39] V.V. Nguyen, G.J. Hancock, C.H. Pham, New developments in the direct strength method (DSM) for the design of cold-formed steel sections under localised loading. Steel Constr. 10 (3) (2017) 227–233.

[40] V.V. Nguyen, G.J. Hancock, C.H. Pham, Analyses of thin-walled sections under localised loading for general end boundary conditions – Part 1: Pre-buckling. Thin-Walled Struct. 119 (2017) 956–972.

[41] V.V. Nguyen, G.J. Hancock, C.H. Pham, Analyses of thin-walled sections under localised loading for general end boundary conditions – Part 2: Buckling. Thin-Walled Struct. 119 (2017) 973–987.

[42] A. Uzzaman, J.B.P. Lim, D. Nash, J. Rhodes, B. Young, Web crippling behaviour of cold-formed steel channel sections with offset web holes subjected to interior two flange loading, Thin-Walled Struct. 50 (2012) 76–86.

[43] A. Uzzaman, J.B.P. Lim, D. Nash, J. Rhodes, B. Young, Cold-formed steel sections with web openings subjected to web crippling under two-flange loading conditions—Part I: tests and finite element analysis, Thin-Walled Struct. 56 (2012) 38–48.

[44] A. Uzzaman, J.B.P. Lim, D. Nash, J. Rhodes, B. Young, Cold-formed steel sections with web openings subjected to web crippling under two-flange loading conditions—Part II: parametric study and proposed design equations, Thin-Walled Struct. 56 (2012) 79–87.

[45] A. Uzzaman, J.B.P. Lim, D. Nash, J. Rhodes, B. Young, Effect of offset web holes on web crippling strength of cold-formed steel channel sections under end-two-flange loading condition, Thin-Walled Struct. 65 (2013) 34–48.

[46] A. Uzzaman, J.B.P. Lim, D. Nash, B. Young, Effects of edge-stiffened circular web openings on the web crippling strength of cold-formed steel channel beams under one-flange loading conditions, Eng. Struct. 139 (2017) 96-107.

[47] A. Uzzaman, J.B.P. Lim, D. Nash, K. Roy, Cold-formed steel channel beams under end-two-flange loading condition: Design for edge-stiffened holes, unstiffened holes and plain webs, Thin-Walled Struct. 147(2020) 106532.

[48] A. Uzzaman, J.B.P. Lim, D. Nash, K. Roy, Web crippling behaviour of cold-formed steel channel sections with edge-stiffened and unstiffened circular holes under interior-two-flange loading condition, Thin-Walled Struct. 154 (2020) 106813.

[49] B.S. Chen, K. Roy, Z.Y. Fang, A. Uzzaman, Y.H. Chi, J.B.P. Lim, Web crippling capacity of fastened cold-formed steel channels with edge-stiffened web holes, un-stiffened web holes and plain webs under two-flange loading, Thin-Walled Struct. (2021) 163.

[50] Rahman. J, Ahmed. K. S, Khan. N. I, Islam. K, & Mangalathu. S, Data-driven shear strength prediction of steel fiber reinforced concrete beams using machine learning approach, Eng. Struct. 233(2021) 111743.

[51] Xie. Y, Ebad. Sichani. M, Padgett. JE, DesRoches. R, The promise of implementing machine learning in earthquake engineering: A state-of-the-art review, Earthquake Spectra, 2020.

[52] S. Mangalathu, J.-S. Jeon, Machine learning–based failure mode recognition of circular reinforced concrete bridge columns: Comparative study, Struct. Eng. 145 (2019).

[53] S. Kameshwar, S. Misra, J.E. Padgett, Decision tree based bridge restoration models for extreme event performance assessment of regional road networks, Struct. Infrastruct. Eng. 16 (2020) 431-451.

[54] Karim. RM, Islam. K, Ahmed. KS, Zhang. Q, Application of machine learning in bridge engineering: a state-of-the-art review. In: Proceedings of the IABSE-JSCE Advances in Bridge Engineering-IV Conference, 2020.

[55] S. Mangalathu, H. Jang, S.-H. Hwang, J.-S. Jeon, Data-driven machine-learning-based seismic failure mode identification of reinforced concrete shear walls, Eng. Struct. 208 (2020).

[56] S. Mangalathu, H. Sun, C.C. Nweke, Z. Yi, H.V. Burton, Classifying earthquake damage to buildings using machine learning, Earthquake Spectra. 36 (1) (2020) 183-208.

[57] Z.Y. Fang, K. Roy, J.B.P. Lim, Deep learning application for web crippling behavior of roll-formed aluminium alloy channel sections with web holes under interior-two-flange loading. ASCE J. Struct. Eng. (under review)

[58] ABAQUS Analysis User's Manual-Version 6.14-2, ABAQUS Inc., USA, 2018.

[59] Y.H. Chi, K. Roy, B.S. Chen, Z.Y. Fang, A. Uzzaman, G.B.G. Ananthi, J.B.P. Lim, Effect of web hole spacing on axial capacity of back-to-back cold-formed steel channels with edge-stiffened holes. Steel Compos. Struct. 40 (2) (2021) 287-305

[60] B.S. Chen, K. Roy, Z.Y. Fang, A. Uzzaman, G. Raftery, J. B. P. Lim, Moment capacity of back-to-back cold-formed steel channels with edge-stiffened holes, un-stiffened holes, and plain webs. Eng. Struct. 235 (2021) 112042.

[61] B.S. Chen, K. Roy, Z.Y. Fang, A. Uzzaman, C. H. Pham, G. Raftery, J. B.P. Lim. Shear behaviour and design cold-formed steel channels with edge -stiffened hole, un-stiffened hole, and plain web. ASCE J. Struct. Eng. 148 (2) (2022) 04021268.

[62] B. Chen, , Roy, K. Uzzaman, A., G.M. Raftery, J. B. P. Lim, Parametric study and simplified design equations for cold-formed steel channels with edge-stiffened holes under axial compression. J. Constr. Steel Res. 172 (2020) 106161.

[63] B. Chen, K. Roy, Uzzaman, A., J. B. P. Lim, Moment capacity of cold-formed channel beams with edge-stiffened web holes, un-stiffened web holes and plain webs, Thin-Walled Struct. 2020, 157, 107070.

[64] K. Roy; J. B. P. Lim, H.H. Lau, P.M. Yong, G.C. Clifton, A. Wrzesien, C.C. Mei, Collapse behavior of a fire engineering designed single-storey cold- formed steel building in severe fires. Thin-Walled Struct. 142 (2019) 340–357.

[65] K. Roy, Lau, H.H., Ting, T.C.H., B. Chen, J. B. P. Lim, Flexural capacity of gapped built-up cold-formed steel channel sections including web stiffeners, J. Constr. Steel Res. 172 (2020) 106154.

[66] K. Roy, B.S. Chen, Z.Y. Fang, A. Uzzaman, X. Chen, J.B.P. Lim. Local and distortional buckling behaviour of back-to-back built-up aluminium alloy channel section columns, Thin-Walled Struct. 163(1) (2021).

[67] K. Roy, B.S. Chen, Z.Y. Fang, A. Uzzaman, J.B.P. Lim, Axial capacity of back-to-back built-up aluminium alloy channel section columns. ASCE J. Struct. Eng. 148 (2) (2022).

[68] K. Roy, T. C. H. Ting, H. H. Lau, J. B. P. Lim, Nonlinear behaviour of back-to-back gapped built-up cold-formed steel channel sections under compression. J. Constr. Steel Res. 147 (2018) 257–276.

[69] Z.Y. Fang, K. Roy, B.S. Chen, Z.X Xie, J.B.P. Lim, Local and distortional buckling behavior of aluminium alloy back-to-back channels with web holes under axial compression. J. Build. Eng. 47 (2022) 103837.

[70] Z.Y. Fang, K. Roy, J. Mares, C.-W. Sham, B.S. Chen, J.B.P. Lim. Deep learning-based axial capacity prediction for cold-formed steel channel sections using Deep Belief Network, Struct. 33 (2021) 2792–2802.

[71] Z.Y. Fang, K. Roy, B.S. Chen, C.-W. Sham, I. Hajirasouliha, J.B.P. Lim. Deep learning-based procedure for structural design of cold-formed steel channel sections with edge-stiffened and un-stiffened holes under axial compression, Thin-Walled Struct. 166 (2021) 108076.

[72] Z.Y. Fang, K. Roy, Y. Chi, B. Chen, J. B.P. Lim, Finite element analysis and proposed design rules for cold-formed stainless steel channels with web holes under end-one-flange loading. Struct. (2021) 2876-2899.

[73] Z.Y. Fang, K. Roy, A. Uzzaman, J. B.P. Lim, Numerical simulation and proposed design rules of cold-formed stainless steel channels with web holes under interior-one-flange loading. Eng. Struct. (2021) 113566.

[74] Z.Y. Fang, K. Roy, Q. Ma, A. Uzzaman, J.B.P. Lim, Application of deep learning method in web crippling strength prediction of cold-formed stainless steel channel sections under end-two-flange loading, Struct. 33 (2021) 2903-2942.

[75] X. Yao, X. Li, Tests and direct strength method on the distortional buckling and interactive buckling of cold-formed thin-walled steel built-up I-section columns under axial compression, Prog. Steel Build. Struct. 23 (12) (2021) 33-46.

[76] Z.Y. Fang, K. Roy, H. Liang, K. Poologanathan, K. Ghosh, A.M.M. Ahmed, J.B.P. Lim, Numerical simulation and design recommendations for web crippling strength of cold-formed Steel channels with web holes under interior-one-flange loading at elevated temperatures. Buildings. 11 (12) (2021) 666.

[77] P. Gatheeshgar, H. Alsanat, K. Poologanathan, S. Gunalan ,N. Degtyareva, I. Hajirasouliha, Web crippling behaviour of slotted perforated cold-formed steel channels: IOF load case, J. Constr. Steel Res. 188 (2022) 106974.

[78] S.J.Qadir, V.B.Nguyen, I.Hajirasouliha, B.Cartwright, M.A.English, Optimal design of cold roll formed steel channel sections under bending considering both geometry and cold work effects, Thin-Walled Struct. 157 (2020) 107020.

[79] J. Ye, S.M. Mojtabaei, I. Hajirasouliha. Local-flexural interactive buckling of standard and optimised cold-formed steel columns, J. Constr. Steel Res. 144 (2018) 106-118.

[80] L. Hsiao, W. Yu, T.V. Galambos, Load and resistance factor design of cold formed steel, calibration of the AISI design provisions, Ninth Progress Report, Civil Engineering Study 88-2, University of Missouri-Rolla, Rolla, Missouri, U.S.A., February 1988.

Notation

a	Hole diameter;
b_w	Overall web depth of section;
b_f	Overall flange width of section;
COV	Coefficient of variation;

E	Young's modulus of elasticity;
Err	Absolute percentage error;
FEA	Finite element analysis;
h	Web flat depth;
ITF	Interior-two-flange;
L	Total length of the channel sections;
MAE	Mean absolute error;
MSE	Mean squared error;
$P_{AS/NZS1664}$	Web crippling strength from AS/NZS 1664.1
$P_{AISI\&AS/NZS}$	Web crippling strength from the AISI & AS/NZS (4600:2018);
P_{CEN}	Web crippling strength from the Eurocode;
P_{EXP}	Web crippling strength from experiments;
P_{FEA}	Web crippling strength from the finite element analysis;
P_p	Prediction value;
P_{prop}	Web crippling strength from the proposed equation;
r	Inside bend radius;
R_{prop}	Web crippling strength reduction factor from the proposed equation;
$R_{Uzzaman}$	Reduction factor from Uzzaman et al.;
R^*	Correlation coefficient;
t	Nominal thickness of the channel section;
t_i	Real output value;
$\bar{t}_i$	Average real output value;
x	Hole distance to bearing block;
y_i	Prediction output value;
$\overline{y_i}$	Average prediction output value;
$\alpha, \beta, \gamma, \lambda, \rho, \mu, \zeta, \zeta$	Equation coefficients;

Lists of tables

Table 1 Comparison of experimental and numerical results

Specimen ID	Web	Length	Bend radius	Thickness	Hole dia	Bearing length	Exp. Load	FEA result	P_{EXP}/P_{FEA}
	d	L	r	t	a	N	P_{EXP}	P_{FEA}	
	(mm)	(mm)	(mm)	(mm)	(mm)	(mm)	(kN)	(kN)	
Unfastened sections									
ITF240-N50-NH-A0-FR	241.75	770	3	1.96	0	50	5.25	5.01	1.05
ITF240-N75-NH-A0-FR	240.78	795	3	1.95	0	75	5.39	5.07	1.06
ITF240-N100-NH-A0-FR	240.35	820	3	1.95	0	100	5.44	5.21	1.05
ITF240-N50-DH-A0.2-FR	241.14	770	3	1.95	48	50	5.06	4.74	1.07
ITF240-N75-DH-A0.2-FR	240.26	795	3	1.95	48	75	5.12	4.86	1.05
ITF240-N100-DH-A0.2-FR	240.93	820	3	1.95	48	100	5.32	4.99	1.07
ITF240-N50-OH-A0.2-FR	241.51	770	3	1.95	48	50	4.82	4.56	1.06
ITF240-N75-OH-A0.2-FR	241.28	795	3	1.95	48	75	4.85	4.69	1.03
ITF240-N100-OH-A0.2-FR	240.27	820	3	1.95	48	100	5.06	4.83	1.05
ITF240-N50-DH-A0.6-FR	240.44	770	3	1.95	144	50	3.81	3.59	1.06
ITF240-N75-DH-A0.6-FR	241.71	795	3	1.96	144	75	3.84	3.77	1.02
ITF240-N100-DH-A0.6-FR	240.54	820	3	1.95	144	100	4.06	3.86	1.05
ITF240-N50-OH-A0.6-FR	241.96	770	3	1.95	144	50	3.5	3.17	1.11
ITF240-N75-OH-A0.6-FR	241.44	795	3	1.95	144	75	3.48	3.3	1.05
ITF240-N100-OH-A0.6-FR	241.15	820	3	1.95	144	100	3.74	3.43	1.09
Average									1.06
Cov									0.02
Fastened sections									
ITF200-N50-NH-A0-FX	240.12	770	3	1.95	0	50	7.63	7.25	1.05
ITF200-N75-NH-A0-FX	240.63	795	3	1.95	0	75	7.68	7.42	1.03
ITF200-N100-NH-A0-FX	241.68	820	3	1.95	0	100	7.99	7.61	1.05
ITF200-N50-DH-A0.2-FX	241.11	770	3	1.96	48	50	7.17	6.99	1.03
ITF200-N75-DH-A0.2-FX	241.45	795	3	1.95	48	75	7.17	7.06	1.02
ITF200-N100-DH-A0.2-FX	241.59	820	3	1.96	48	100	7.44	7.31	1.02
ITF200-N50-OH-A0.2-FX	241.68	770	3	1.96	48	50	7.1	6.86	1.03
ITF200-N75-OH-A0.2-FX	241.43	795	3	1.96	48	75	7.21	7.04	1.02
ITF200-N100-OH-A0.2-FX	241.1	820	3	1.96	48	100	7.6	7.21	1.05
ITF200-N50-DH-A0.6-FX	241.79	770	3	1.94	144	50	4.98	4.92	1.01
ITF200-N75-DH-A0.6-FX	241.51	795	3	1.94	144	75	5.1	5.11	1
ITF200-N100-DH-A0.6-FX	241.13	820	3	1.94	144	100	5.41	5.37	1.01
ITF200-N50-OH-A0.6-FX	241.83	770	3	1.95	144	50	5.84	5.4	1.08
ITF200-N75-OH-A0.6-FX	240.69	795	3	1.95	144	75	5.87	5.54	1.06
ITF200-N100-OH-A0.6-FX	240.53	820	3	1.95	144	100	6.36	5.74	1.11
Average									1.04
Cov									0.03

Table 2 Performance measure of developed machine learning model

XGBoost Training			XGBoost Testing		
*R**	RMSE	MAE	*R**	RMSE	MAE
0.9998	0.0057	0.0033	0.9969	0.5341	0.2442

Table 3 Cross-validation with linear regression and random forest regression analysis results

Methods	XGBoost	Random Forest	Linear Regression
Cross_validation_Score	0.996786	0.992931	0.902183
NMSE	-0.288674	-0.622938	-8.486916

Table 4 Absolute percentage error for numerical failure load

Specimen ID	Web	Length	Hole dia	Bearing length	Failure load	Err% (AS/NZS1664)	Err% (EC)	Err% (AISI&AS/NZS)	Err (XGBoost)
	d	*L*	*a*	*N*	P_{FEA}				
	(mm)	(mm)	(mm)	(mm)	(kN)				
Unlipped channels with un-fastened flanges									
1 ITF240-N50-NH-A0-FR	240	746	0	50	28.07	74.08	84.35	64.72	5.59
2 ITF240-N75-NH-A0-FR	240	771	0	75	28.66	71.52	83.11	63.09	5.68
3 ITF240-N100-NH-A0-FR	240	796	0	100	29.43	69.01	82.13	61.83	3.49
4 ITF240-N50-DH-A0.2-FR	240	746	46.4	50	25.97	--	--	--	5.14
5 ITF240-N75-DH-A0.2-FR	240	771	46.4	75	26.53	--	--	--	6.2
6 ITF240-N100-DH-A0.2-FR	240	796	46.4	100	27.25	--	--	--	5.17
7 ITF240-N50-OH-A0.2-FR	240	746	46.4	50	26.33	--	--	--	8.1
8 ITF240-N75-OH-A0.2-FR	240	771	46.4	75	27	--	--	--	7.43
9 ITF240-N100-OH-A0.2-FR	240	796	46.4	100	27.81	--	--	--	6.55
10 ITF240-N50-DH-A0.6-FR	240	746	139.2	50	17.38	--	--	--	4.4
11 ITF240-N75-DH-A0.6-FR	240	771	139.2	75	18.23	--	--	--	5.87
12 ITF240-N100-DH-A0.6-FR	240	796	139.2	100	19.16	--	--	--	5.13
13 ITF240-N50-OH-A0.6-FR	240	746	139.2	50	19.22	--	--	--	7.68
14 ITF240-N75-OH-A0.6-FR	240	771	139.2	75	19.96	--	--	--	5.32
15 ITF240-N100-OH-A0.6-FR	240	796	139.2	100	20.77	--	--	--	6.46
Average						71.54	83.2	63.21	5.88
Cov						2.07	0.91	1.19	1.19
Unlipped channels with fastened flanges									
16 ITF240-N50-NH-A0-FX	240	746	0	50	28.07	71.09	82.55	68.91	6.59
17 ITF240-N75-NH-A0-FX	240	771	0	75	28.66	67.71	80.84	67.79	6.55
18 ITF240-N100-NH-A0-FX	240	796	0	100	29.43	65.15	79.9	67.61	8.49
19 ITF240-N50-DH-A0.2-FX	240	746	46.4	50	25.97	--	--	--	7.14
20 ITF240-N75-DH-A0.2-FX	240	771	46.4	75	26.53	--	--	--	5.2
21 ITF240-N100-DH-A0.2-FX	240	796	46.4	100	27.25	--	--	--	6.17
22 ITF240-N50-OH-A0.2-FX	240	746	46.4	50	26.33	--	--	--	8.1
23 ITF240-N75-OH-A0.2-FX	240	771	46.4	75	27	--	--	--	5.43
24 ITF240-N100-OH-A0.2-FX	240	796	46.4	100	27.81	--	--	--	5.55
25 ITF240-N50-DH-A0.6-FX	240	746	139.2	50	17.38	--	--	--	7.4
26 ITF240-N75-DH-A0.6-FX	240	771	139.2	75	18.23	--	--	--	5.87
27 ITF240-N100-DH-A0.6-FX	240	796	139.2	100	19.16	--	--	--	5.13
28 ITF240-N50-OH-A0.6-FX	240	746	139.2	50	19.22	--	--	--	5.68
29 ITF240-N75-OH-A0.6-FX	240	771	139.2	75	19.96	--	--	--	5.32
30 ITF240-N100-OH-A0.6-FX	240	796	139.2	100	20.77	--	--	--	7.46
Average						67.98	81.1	68.1	6.41
Cov						2.44	1.1	0.57	1.06

Table 5 Web crippling strength reduction factors (R) of RFA unlipped channels

Flange type / Hole location		R	
		Un-fastened flanges	Fastened flanges
Centre hole	a/h=0.2	0.95	0.96
	a/h=0.4	0.85	0.87
	a/h=0.6	0.74	0.75
	a/h=0.8	0.57	0.59
Offset hole	a/h=0.2	0.93	0.95
	a/h=0.4	0.80	0.86
	a/h=0.6	0.67	0.76
	a/h=0.8	0.53	0.65

Table 6 Coefficients of web crippling strength formulae

	Support and Flange conditions	C	C_R	C_N	C_h
$h/t<60$	Unfastened to support	15.980	0.184	0.073	0.050
	Fastened to support	16.411	0.247	0.156	0.047
$h/t\geq60$	Unfastened to support	14.564	0.095	0.048	0.048
	Fastened to support	19.252	0.131	0.065	0.047

Table 7 Coefficients for web crippling strength reduction factor formulae

Coefficient	Flange unfastened to support	Flange fastened to support
α	1.072	1.082
γ	0.623	0.609
λ	0.040	0.027
β	0.968	0.950
μ	0.617	0.438
ζ	0.077	0.052
ξ	0.099	0.125

Table 8 Comparisons of web crippling strengths obtained from FEA and current design rules

Specimen ID	Failure load P_{FEA} (kN)	$P_{FEA}/P_{AS/NZS1664}$	P_{FEA}/P_{CEN}	$P_{FEA}/P_{AISI\&AS/NZS}$	$P_{FEA}/P_{pro\,p}$	$R_{FEA}/P_{Uzzaman}$	$R_{FEA}/P_{pro\,p}$
Plain unlipped channels with un-fastened flanges							
ITF240-N50-NH-A0-FR	28.07	0.69	1.14	0.51	1.08	--	--
ITF240-N75-NH-A0-FR	28.66	0.62	1.05	0.48	1.05	--	--
ITF240-N100-NH-A0-FR	29.43	0.57	0.99	0.46	1.04	--	--
Average		0.63	1.06	0.48	1.06	--	--
Cov		0.05	0.06	0.02	0.02	--	--
Plain sections with fastened flanges						--	--
ITF200-N50-NH-A0-FX	36.43	0.89	1.48	0.83	1.12	--	--
ITF200-N75-NH-A0-FX	36.99	0.80	1.35	0.80	1.05	--	--
ITF200-N100-NH-A0-FX	38.22	0.74	1.29	0.80	1.03	--	--
Average		0.81	1.37	0.81	1.07	--	--
Cov		0.06	0.08	0.01	0.04	--	--
Perforated unlipped channels with un-fastened flanges							
ITF240-N50-DH-A0.2-FR	1.27	--	--	--	--	0.98	0.98
ITF240-N75-DH-A0.2-FR	1.43	--	--	--	--	0.98	0.97
ITF240-N100-DH-A0.2-FR	1.54	--	--	--	--	0.98	0.96
ITF240-N50-OH-A0.2-FR	1.44	--	--	--	--	--	1.02
ITF240-N75-OH-A0.2-FR	1.59	--	--	--	--	--	1.02
ITF240-N100-OH-A0.2-FR	1.75	--	--	--	--	--	1.02
ITF240-N50-DH-A0.6-FR	0.79	--	--	--	--	0.85	0.85
ITF240-N75-DH-A0.6-FR	0.89	--	--	--	--	0.87	0.87
ITF240-N100-DH-A0.6-FR	0.98	--	--	--	--	0.89	0.88
ITF240-N50-OH-A0.6-FR	1.13	--	--	--	--	--	1.04
ITF240-N75-OH-A0.6-FR	1.27	--	--	--	--	--	1.05
ITF240-N100-OH-A0.6-FR	1.41	--	--	--	--	--	1.05
Average		--	--	--	--	0.93	0.98
Cov		--	--	--	--	0.06	0.07
Perforated unlipped channels with fastened flanges							
ITF200-N50-DH-A0.2-FX	2.16	--	--	--	--	0.99	0.94
ITF200-N75-DH-A0.2-FX	2.46	--	--	--	--	0.99	0.95
ITF200-N100-DH-A0.2-FX	2.84	--	--	--	--	0.98	0.94
ITF200-N50-OH-A0.2-FX	2.45	--	--	--	--	--	1.01
ITF200-N75-OH-A0.2-FX	2.84	--	--	--	--	--	1.00
ITF200-N100-OH-A0.2-FX	3.24	--	--	--	--	--	1.00
ITF200-N50-DH-A0.6-FX	1.5	--	--	--	--	0.86	0.85
ITF200-N75-DH-A0.6-FX	1.73	--	--	--	--	0.89	0.87
ITF200-N100-DH-A0.6-FX	1.97	--	--	--	--	0.90	0.89
ITF200-N50-OH-A0.6-FX	2.13	--	--	--	--	--	0.96
ITF200-N75-OH-A0.6-FX	2.53	--	--	--	--	--	0.97
ITF200-N100-OH-A0.6-FX	2.9	--	--	--	--	--	0.97
Average		--	--	--	--	0.94	0.95
Cov		--	--	--	--	0.05	0.05

Table 9 Reliability analysis results

(a) For web crippling strength equations

Section type	Unfastened section	Fastened section
Ratio of equations	P_{FEA} / P_{prop}	P_{FEA} / P_{prop}
Data number	108	108
Mean, P_m	1.02	1.03
β' [17]	3.41	3.62
φ [17]	0.85	0.85

(b) For web crippling strength reduction factor equations

Section type	Unfastened section	Fastened section
Ratio of equations	R_{FEA} / R_{prop}	R_{FEA} / R_{prop}
Data number	432	432
Mean, P_m	1.00	1.00
β' [17]	3.61	3.61
φ [17]	0.85	0.85

List of Figures

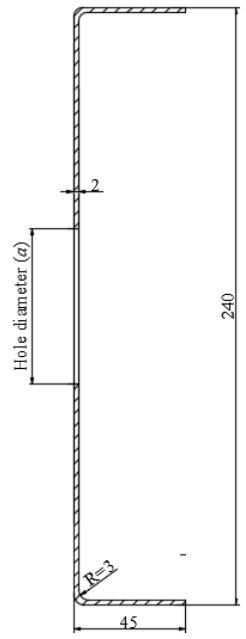

(a) Nominal cross-section of investigated channel (All dimensions are in mm)

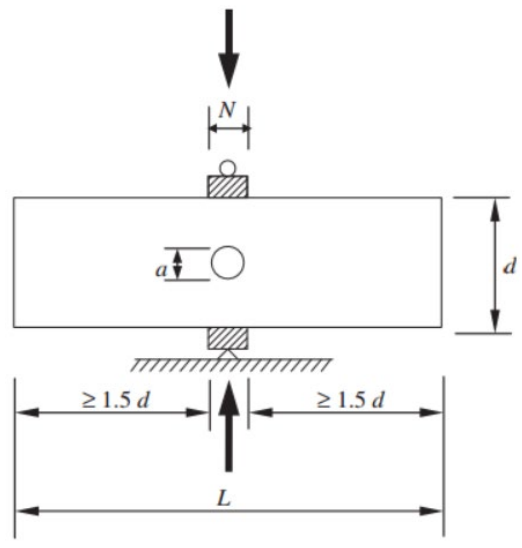

(b) ITF loading condition with centred web hole

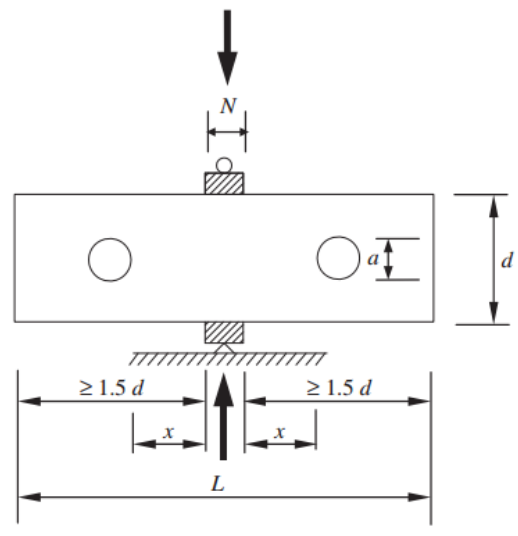

(c) ITF loading condition with offset web hole

Fig.1 Cross-section dimension and loading condition

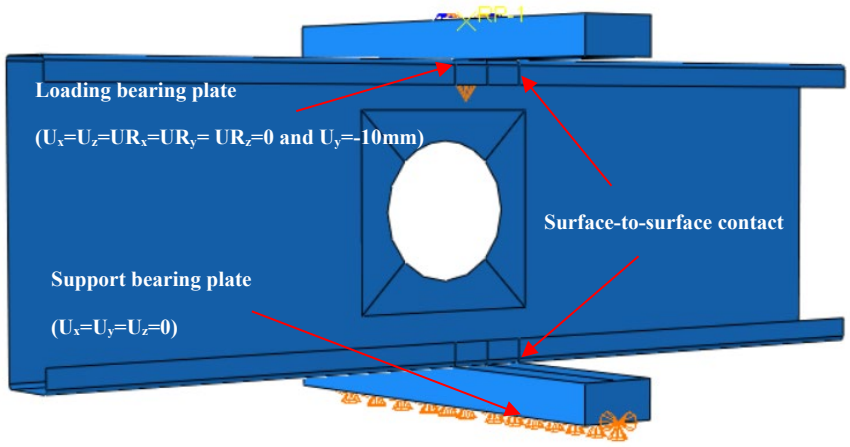

(a) Boundary conditions used in FE model with lipped channel

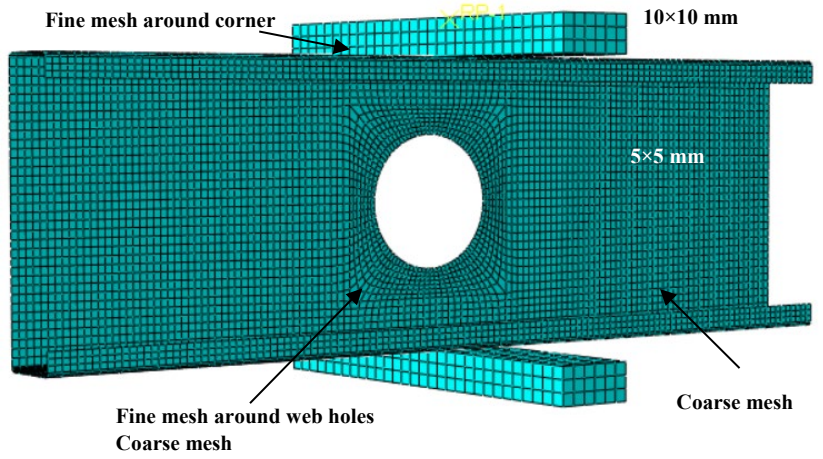

(b) Meshing for FE model with lipped channel

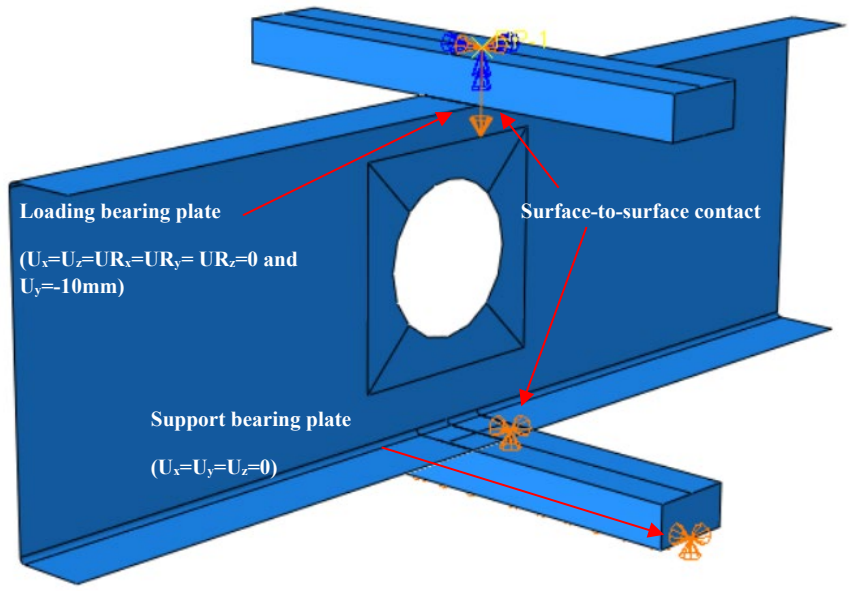

(c) Boundary conditions used in FE model with unlipped channel

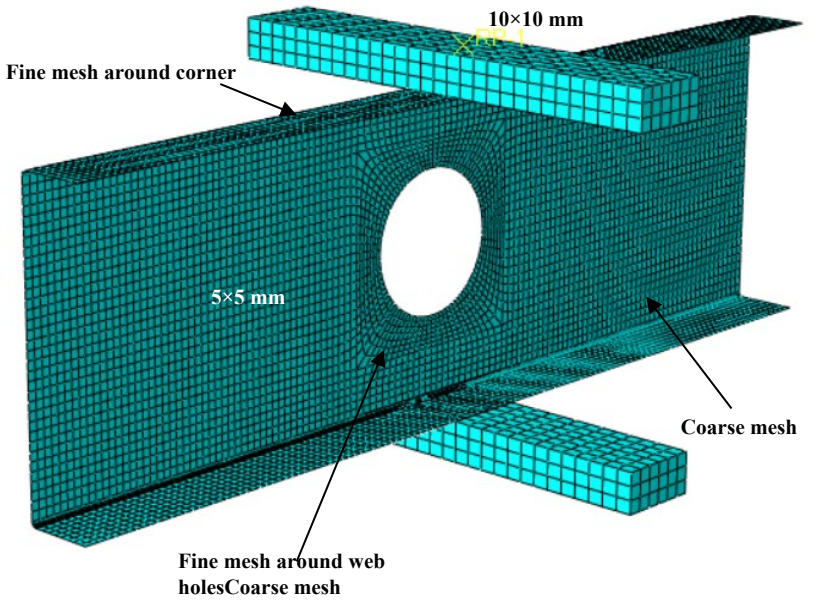

(d) Meshing for FE model with unlipped channel

Fig.2 Details of FE model

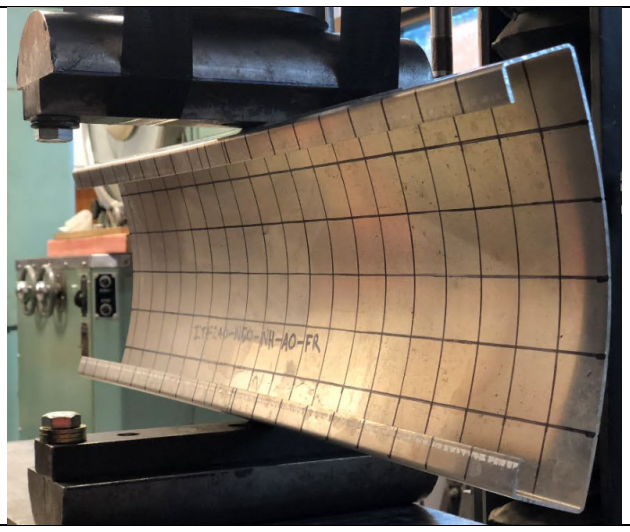

(i) Test

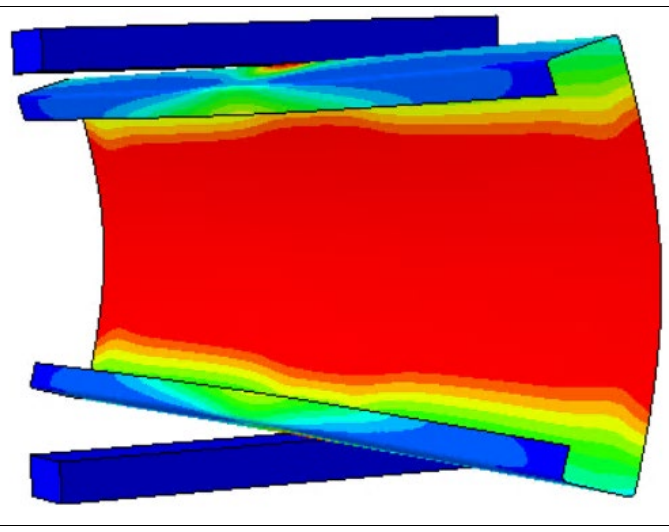

(ii) FEA

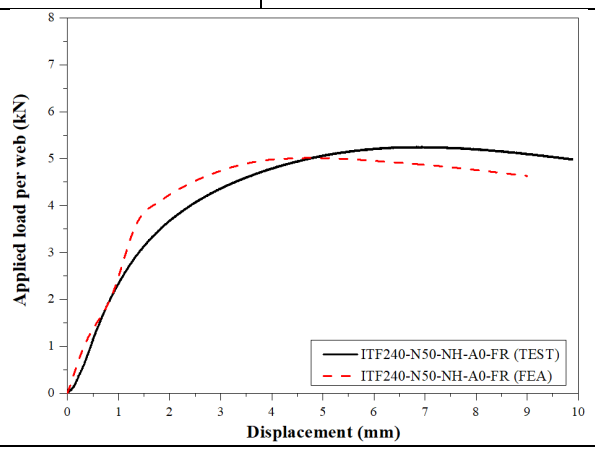

(iii) Web deformation curves

(a) ITF240-N50-NH-A0-FR

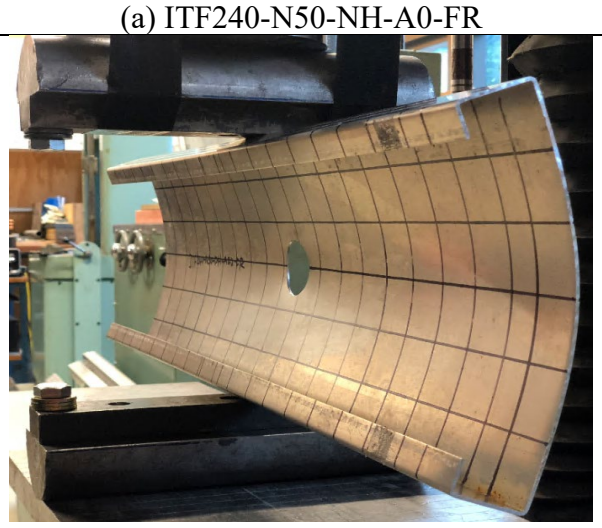

(i) Test

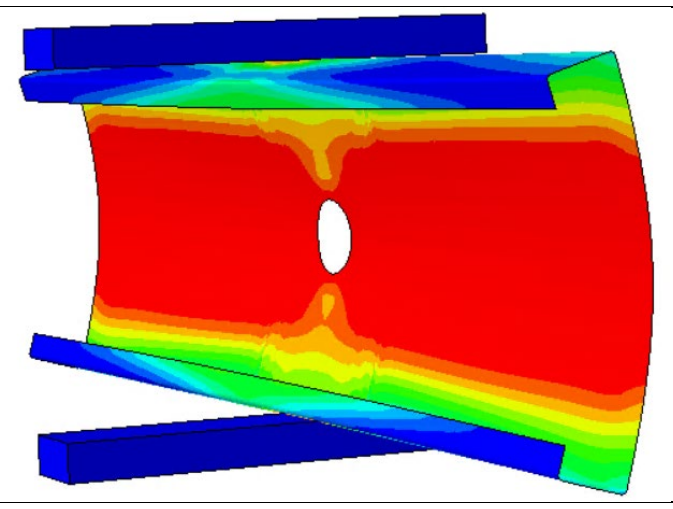

(ii) FEA

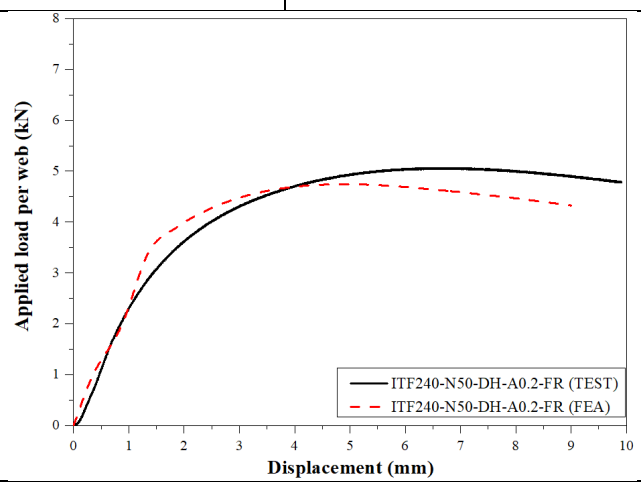

(iii) Load-displacement curve

(b) ITF240-N50-DH-A0.2-FR

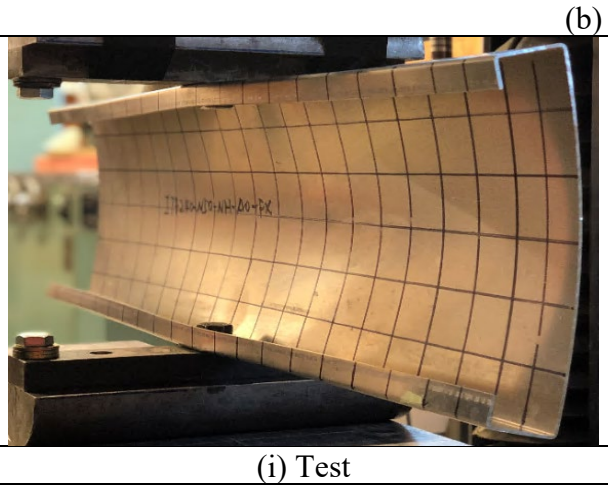

(i) Test

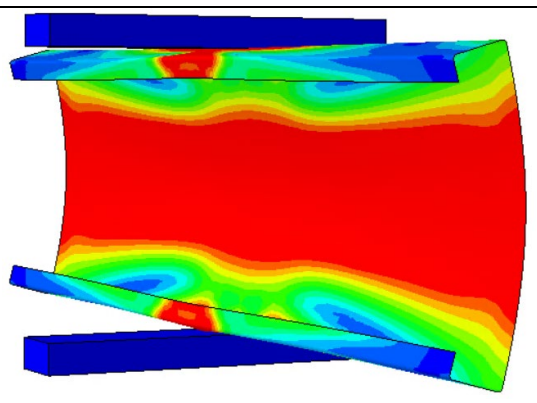

(ii) FEA

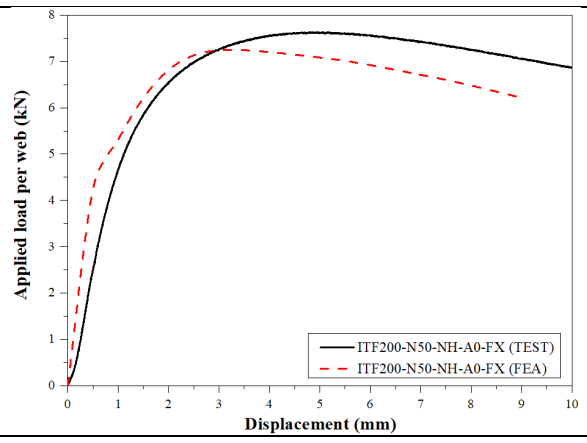

(iii) Load-displacement curve

(c) ITF200-N50-NH-A0-FX

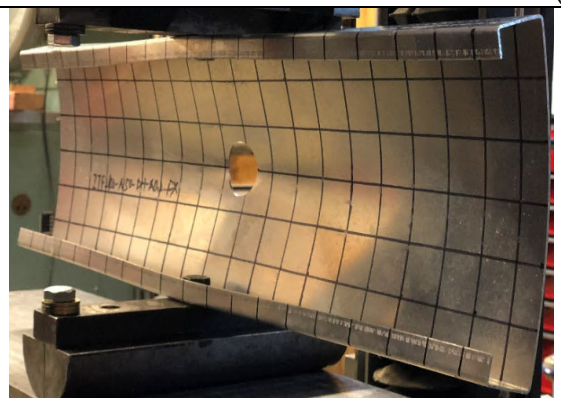

(i) Test

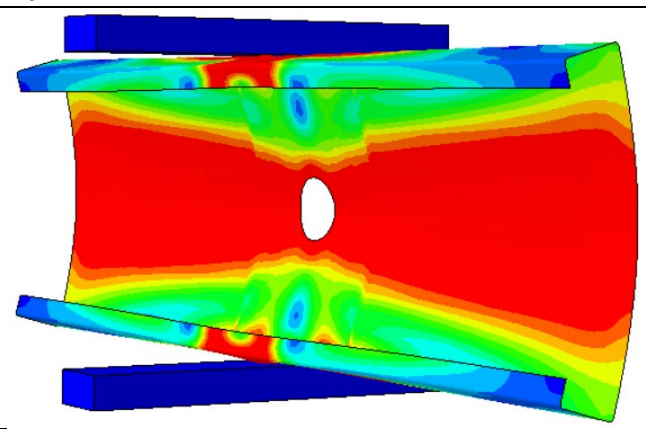

(ii) FEA

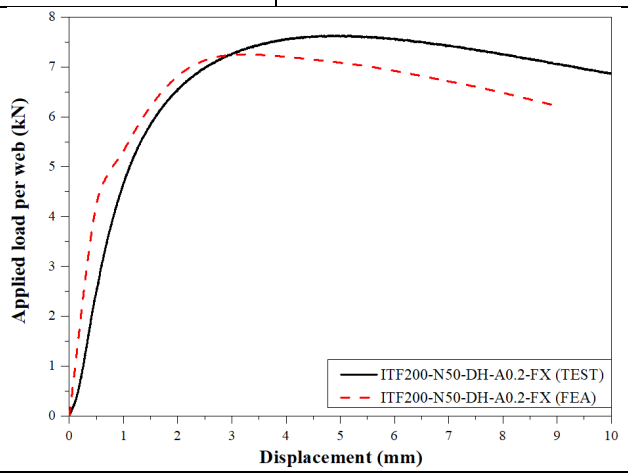

(iii) Load-displacement curve

(d) ITF200-N50-DH-A0.2-FX

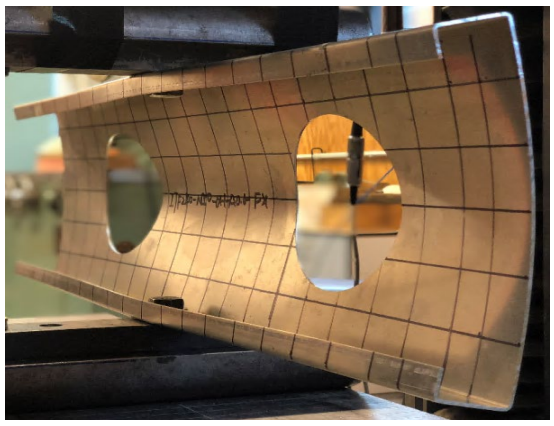

(i) Test

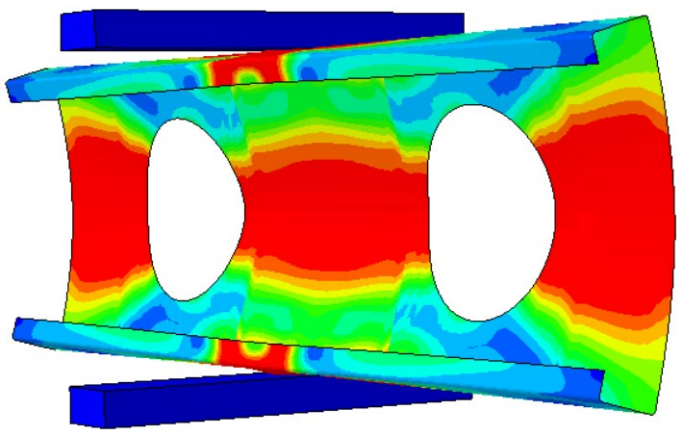

(ii) FEA

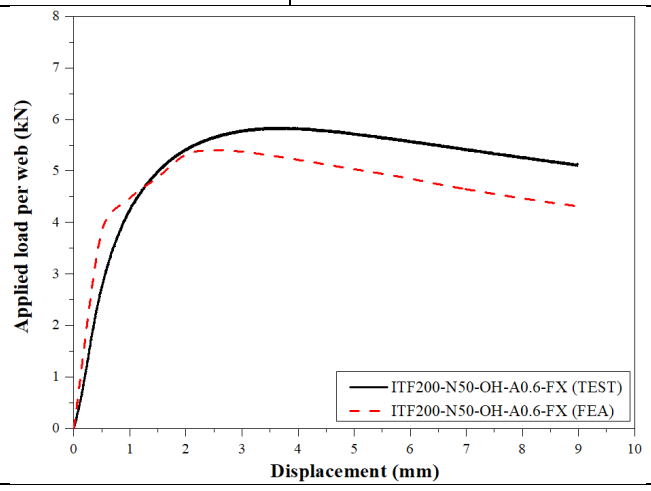

(iii) Load-displacement curve

(e) ITF200-N50-OH-A0.6-FX

Fig.3 Validation of FE model [57]

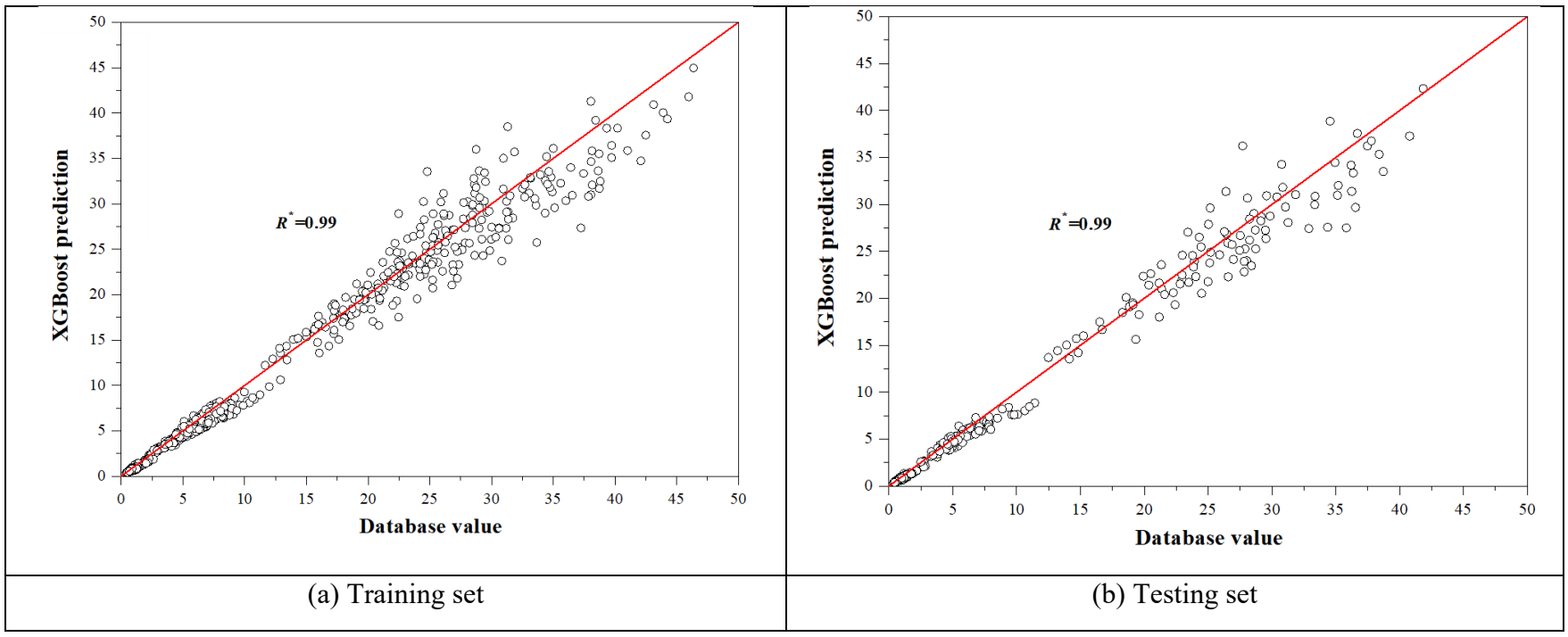

(a) Training set

(b) Testing set

Fig.4 XGBoost training

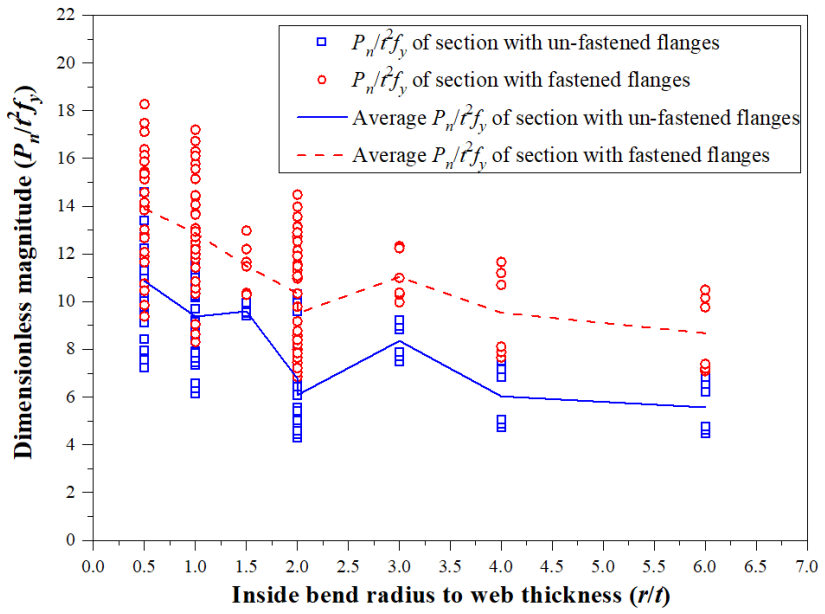

(a) Effect of r/t

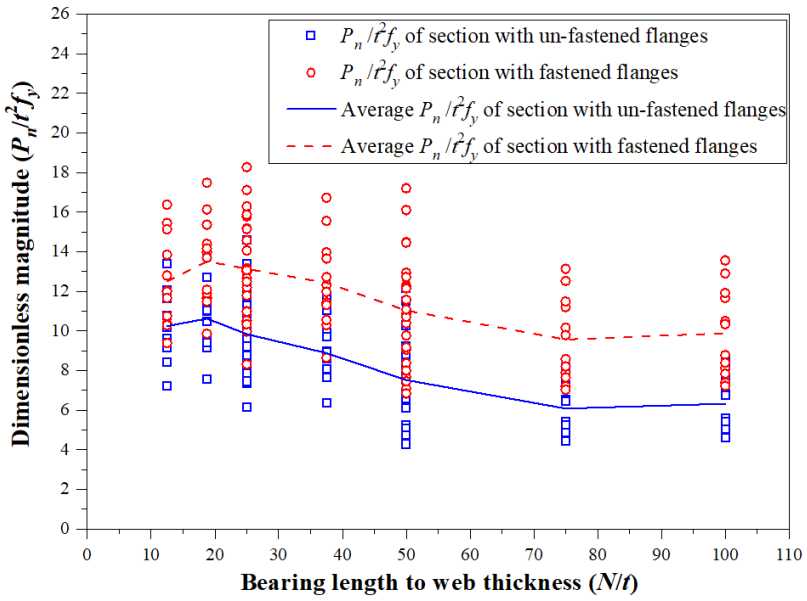

(b) Effect of N/t

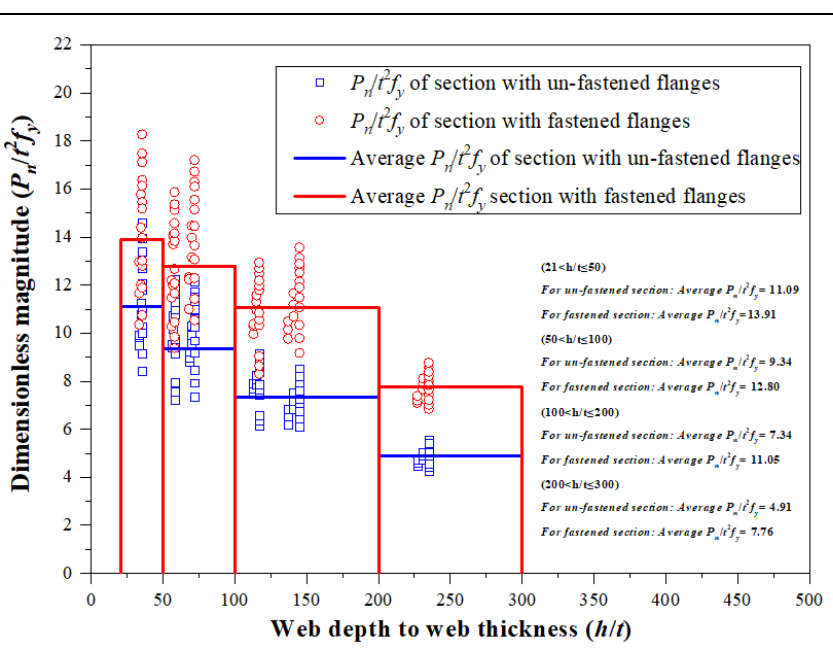

(c) Effect of h/t

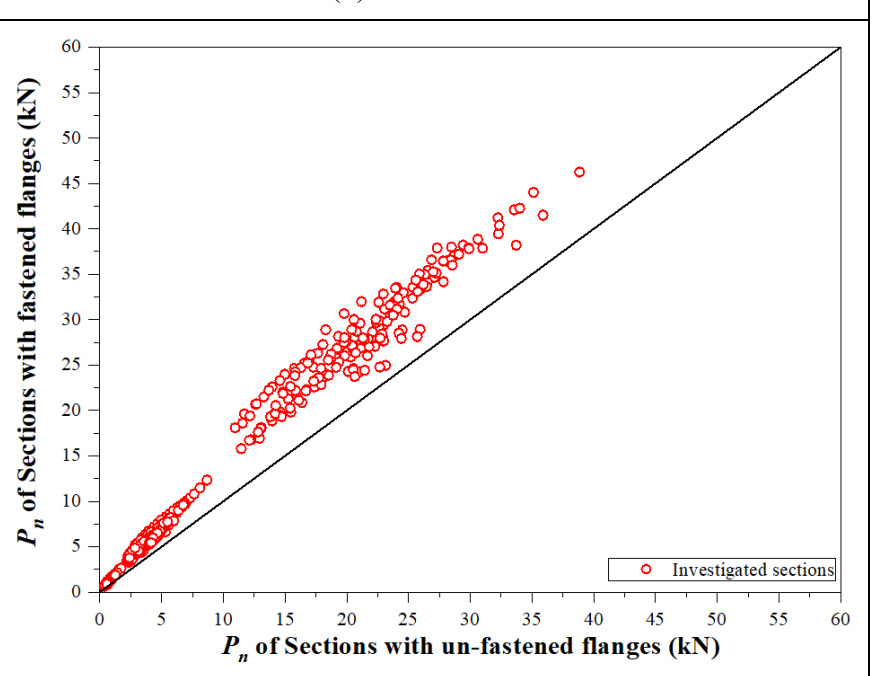

(d) Effect of flange type

Fig.5 Effect of r/t, N/t, h/t and flange type

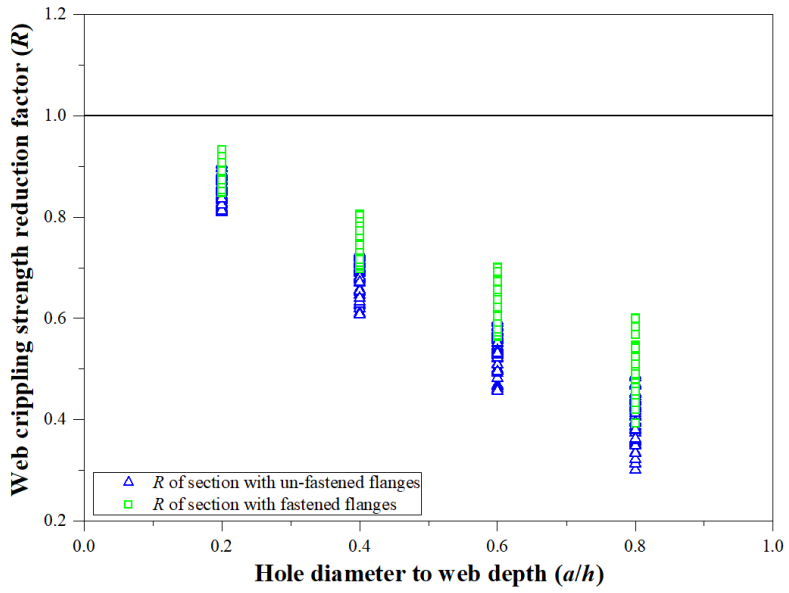

(i) RFA unlipped channels with centred web hole

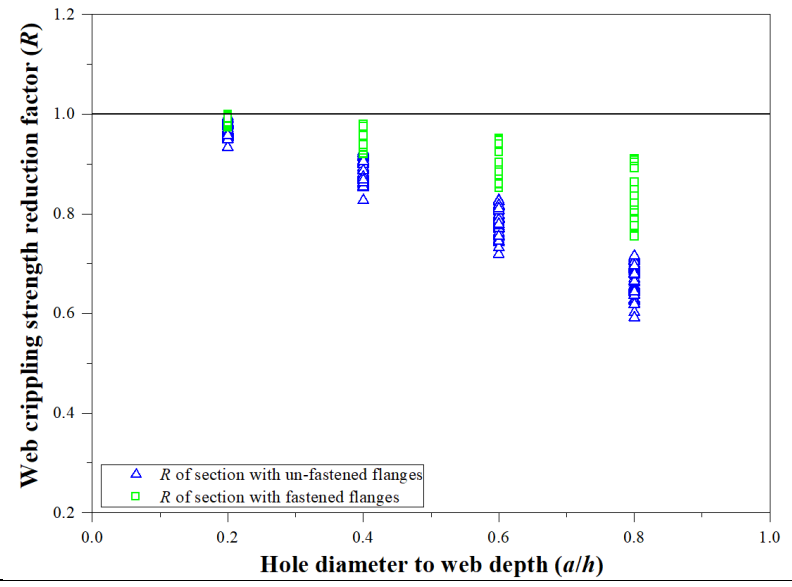

(ii) RFA unlipped channels with offset web holes

(a) Effect of *a/h*

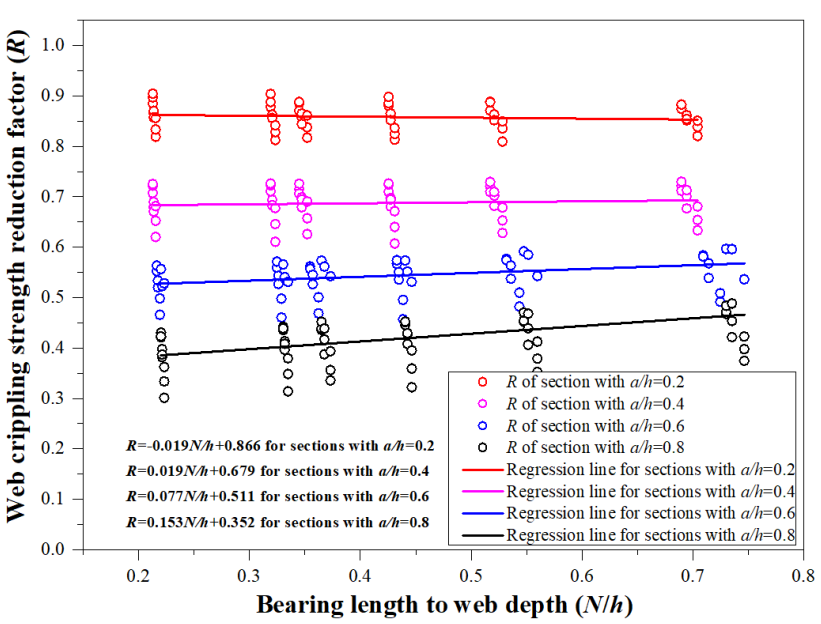

(i) RFA unlipped channels with un-fastened flanges and centred web holes

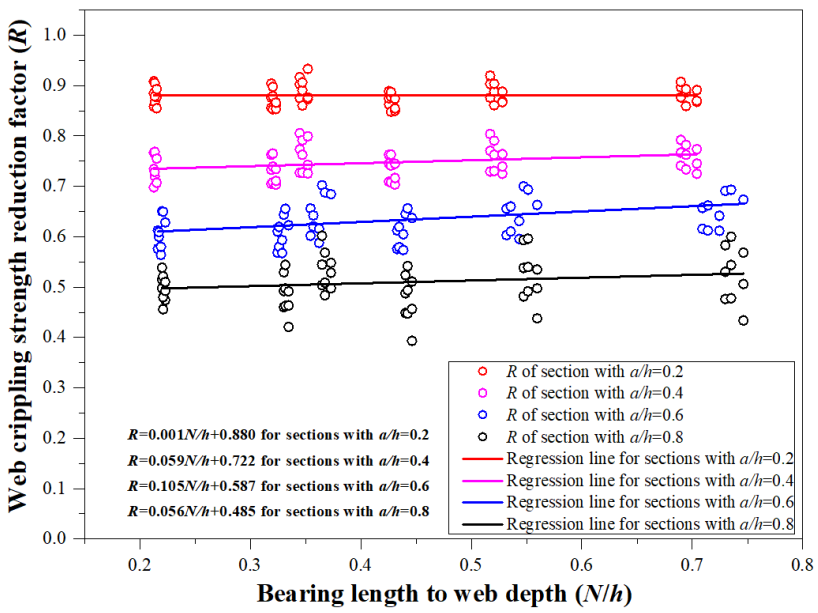

(ii) RFA unlipped channels with fastened flanges and centred web holes

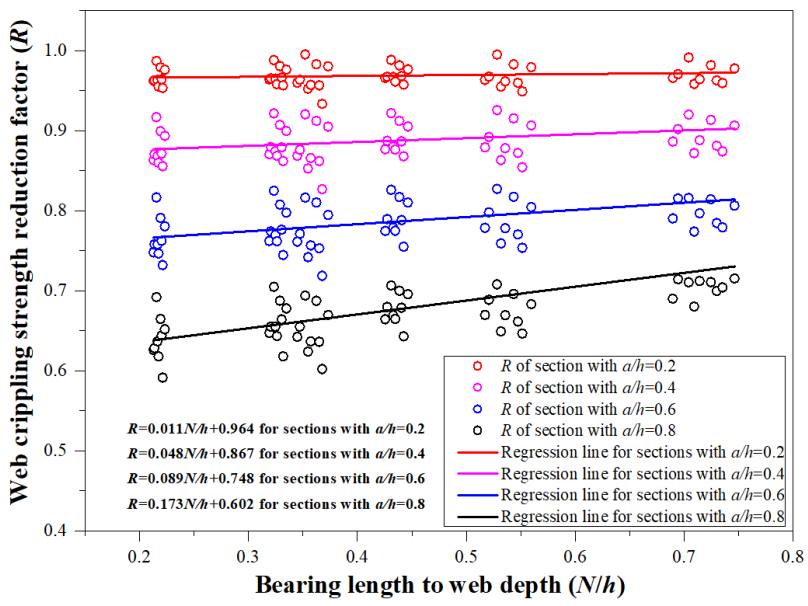

(iii) RFA unlipped channels with un-fastened flanges and offset web holes

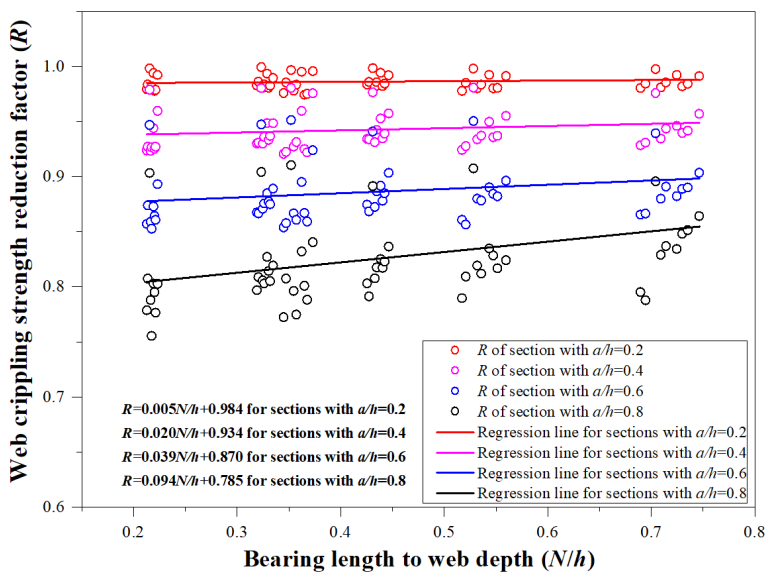

(iv) RFA unlipped channels with fastened flanges and offset web holes

(b) Effect of *N/h*

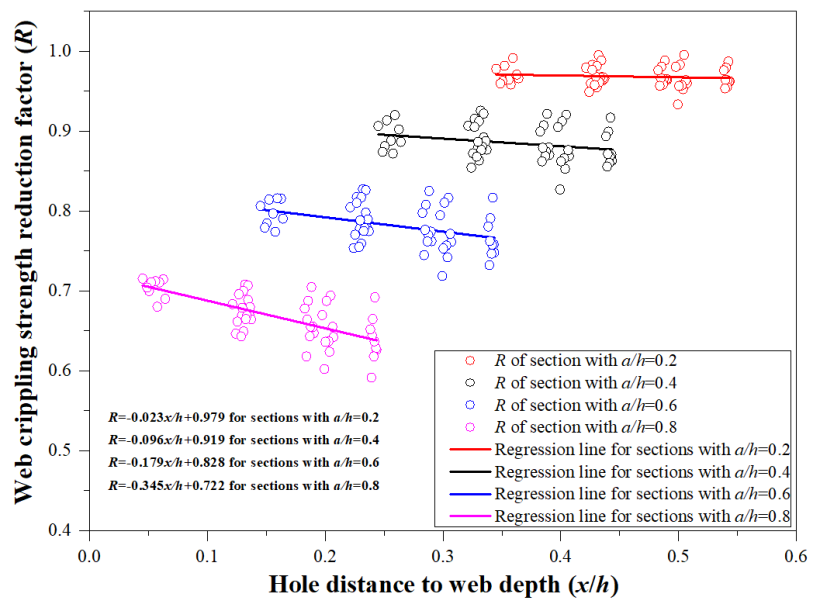

(i) RFA unlipped channels with un-fastened flanges and offset web holes

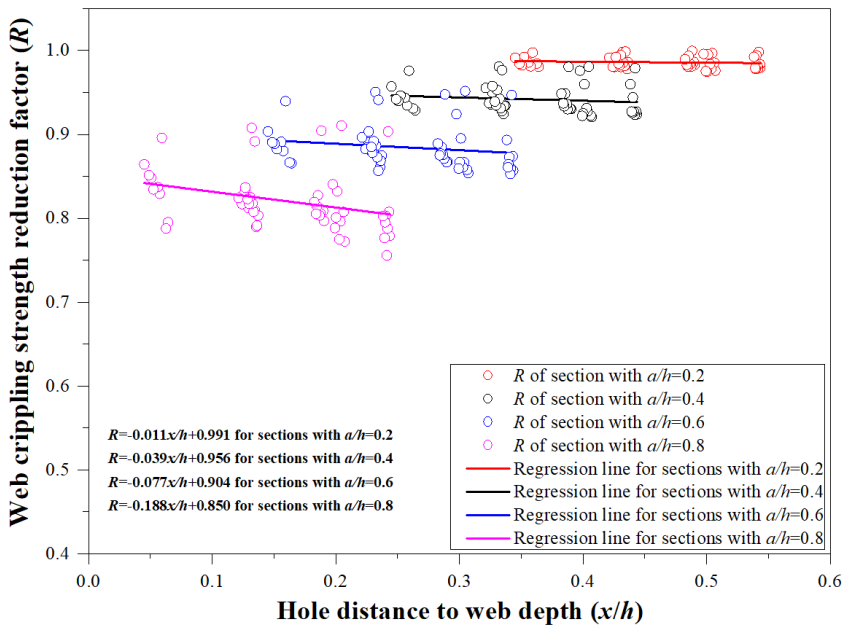

(ii) RFA unlipped channels with fastened flanges and offset web holes

(c) Effect of x/h

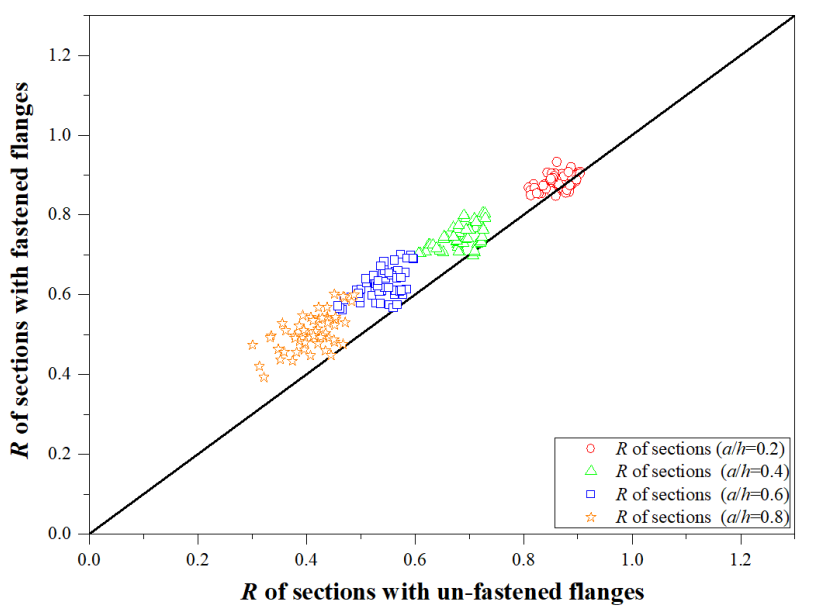

(i) RFA unlipped channels with centred web holes

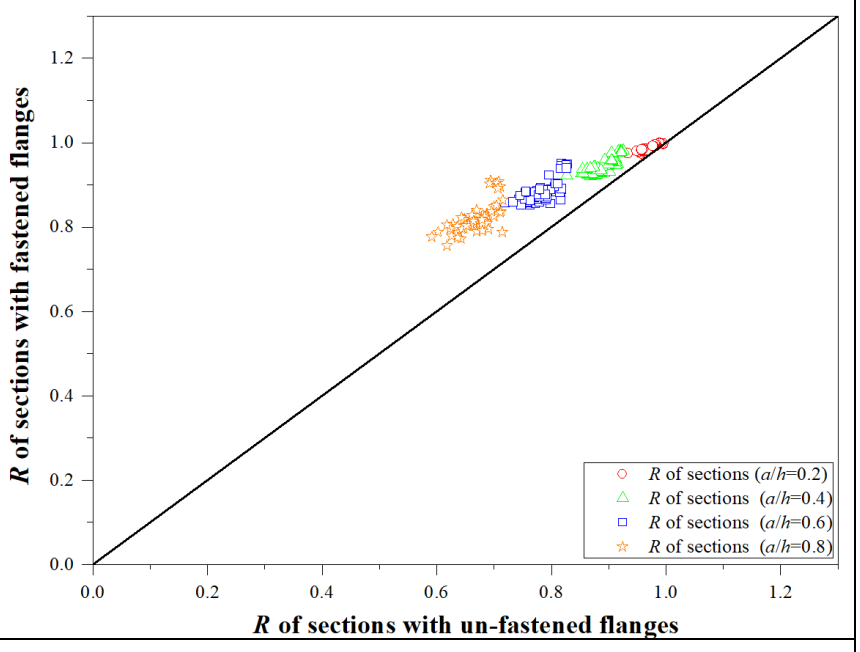

(ii) RFA unlipped channels with offset web holes

(d) Effect of flange type

Fig.6 Effect of a/h, N/h, x/h and flange type